AIAA 98-0905
HSCT Configuration Design Using Response Surface Approximations of Supersonic Euler Aerodynamics

Knill, D.L., Giunta, A.A., Baker, C.A., Grossman, B., Mason, W.H., Haftka, R.T. and Watson, L.T.

Virginia Polytechnic Institute and State University, Blacksburg, VA

36th Aerospace Sciences Meeting & Exhibit
January 12-15, 1998 / Reno, NV

Multidisciplinary HSCT Design Using Response Surface Approximations of Supersonic Euler Aerodynamics

Duane L. Knill*, Anthony A. Giunta†, Chuck A. Baker‡, Bernard Grossman§, William H. Mason¶, Raphael T. Haftka‖, and Layne T. Watson**

Multidisciplinary Analysis and Design Center for Advanced Vehicles
Virginia Polytechnic Institute and State University
Blacksburg, Virginia 24061–0203

Abstract

A method has been developed to efficiently implement supersonic aerodynamic predictions from Euler solutions into a highly constrained, multidisciplinary design optimization of a High-Speed Civil Transport (HSCT) configuration. The method alleviates the large computational burden associated with performing CFD analyses and eliminates the numerical noise present in the analyses through the use of response surface (RS) methodologies, a variation of the variable-complexity modeling (VCM) technique, and coarse grained parallel computing. Variable-complexity modeling techniques allow one to take advantage of information gained from inexpensive lower fidelity models while maintaining the accuracy of the more expensive high fidelity methods. In this research, simple conceptual level aerodynamic models provide the functional form of the drag polar. Response surface models are therefore created for the intervening functions (drag polar shape parameters) revealed by the simple models instead of for the drag itself. Optimization results using linear theory RS models are used to select the allowable ranges of the design variables. Stepwise regression analysis, performed using data from linear theory aerodynamic results, provides information on the relative importance of each term in the polynomial RS models. With this information, reduced term RS models representing a correction to the linear theory RS model predictions are constructed using fewer Euler evaluations. Studies into five, ten, fifteen, and twenty variable HSCT design problems show that accurate results can be obtained with the reduced term models at a fraction of the cost of creating the full term quadratic RS models. Specifically, 11 hour, 47 hour, 115 hour, and 255 hour savings in CPU time on a single 75 MHz IP21 processor of a SGI *Power Challenge* are obtained for the five, ten, fifteen, and twenty variable design problems, respectively. Errors in the RS model cruise drag predictions, based on actual Euler calculations, for the optimal designs range from 0.1 counts to 0.8 counts for the twenty variable optimum.

1. Introduction

With advances in computational fluid dynamics (CFD) code maturity, grid generation capabilities, and computer performance, the application of CFD in the aircraft design process[1] has received much attention. Introducing accurate CFD predictions in the early stages of design has a large potential advantage in terms of aircraft life cycle cost and time-to-market. According to Nicolai,[2] about eighty percent of the aircraft life cycle cost is set after the conceptual design stage. Using more accurate aerodynamic predictions early in the design process, when the aircraft is taking shape, can result in less time and money spent in redesign and an overall improved product. However, the relatively large computational expense associated with CFD analyses can discourage its application in high dimensional design optimization procedures. A new procedure must be developed to enable the efficient implementation of aerodynamic predictions from CFD solutions into high dimensional, highly constrained MDO procedures.

Previous work performed at Virginia Tech[3–6] tackled the computational expense problem by employing a *variable-complexity modeling* (VCM) technique to the multidisciplinary design optimization (MDO) of a High-Speed Civil Transport (HSCT) configuration (Fig. 1). This technique utilized both conceptual level and preliminary level models for predicting aerodynamic performance and structural weights. The simple conceptual design level methods (algebraic relations) were used predominantly in the optimization due to their low computational costs. More accurate

*Graduate Research Assistant, Dept. of Aerospace and Ocean Engineering. Current Position: Postdoctoral Research Associate, Dept. of Aeronautics and Astronautics, University of Washington, Seattle, WA, Member AIAA.

†Postdoctoral Research Associate, National Research Council/NASA Langley Research Center, Hampton, VA, Member AIAA.

‡Graduate Research Assistant, Dept. of Aerospace and Ocean Engineering, Student Member AIAA.

§Professor and Dept. Head of Aerospace and Ocean Engineering, Associate Fellow AIAA.

¶Professor of Aerospace and Ocean Engineering, Associate Fellow AIAA.

‖Professor of Aerospace Engineering, Mechanics and Engineering Science, University of Florida, Gainesville, FL, Fellow AIAA

**Professor of Computer Science and Mathematics

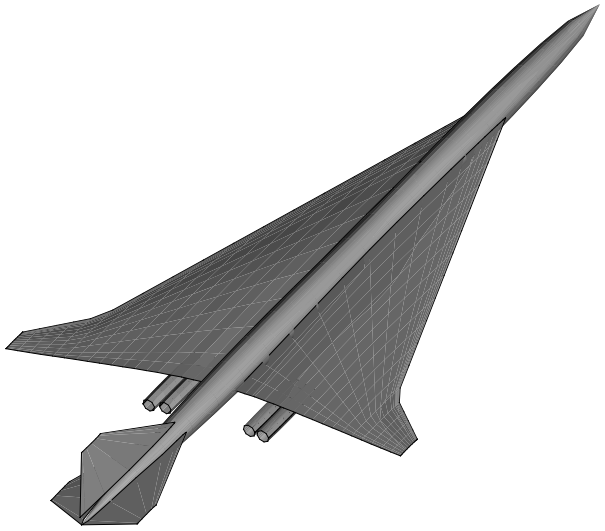

Figure 1: Typical HSCT Configuration.

and more computationally expensive methods (linear theory aerodynamics and structural optimization) are used to periodically update the simpler models. In this way, one incorporates the accuracy of the higher level codes with the computational efficiency of the simpler models.

This procedure was effective in reducing the computational cost, but it was still plagued by poor convergence and the appearance of artificial local minima. These problems were a result of high frequency, low amplitude variations in the results from aerodynamic and structural analyses. This *numerical noise* is present in any method with iterative procedures or discrete representations of continuous geometric shapes or physical phenomena.[7,8] Low amplitude, high frequency oscillations have been found in wave drag predictions from slender body theory[7] and in panel level drag-due-to-lift results.[9] Numerical noise can also result from suboptimizations which are performed within the complete optimization framework. Balabanov[10] *et al.* show such noise from structural optimization and wing camber optimization procedures.

Response surface modeling techniques for aerodynamic and structural design improve the performance of highly constrained gradient based optimizations.[7,10,12,13] Using RS models offers a number of benefits. First, the RS models smooth out numerical noise present in the analyses, improving the performance of the gradient based optimizer and eliminating artificial local minima. Second, the analysis codes are separated from the optimization routines. This eliminates problems associated with integrating large production level grid generators, analysis codes, and post processing utilities with the optimizer. It also allows analyses to be performed by experts in the specific discipline on parallel architecture machines. Aspects of the parallel computing performed in this research is presented in Appendix B.

Modeling a complex response, such as the aircraft drag, in high dimensional design spaces via polynomial RS models is difficult because the accuracy of RS models often degrades with the dimension, and the cost of creating RS models increases rapidly with the dimension of the problem. Response surfaces must overcome these problems associated with the *curse of dimensionality*. As the dimension of the problem increases, the number of terms in a quadratic polynomial RS model increase quadratically. The number of design point evaluations required to accurately model the polynomial terms, and the associated computational expense, grows even faster. Balabanov[11] dealt with this by applying constant and linear *corrections* to the lower fidelity RS models in order to create RS models for detailed level structural optimization results. Another issue in the curse of dimensionality is that the accuracy of the RS models tends to degrade as the dimension increases. Due to computational expense issues, the distribution of design points used to evaluate the polynomial becomes quite sparse in large dimensional design boxes. Another contributing factor to the degradation in the RS model fit is the fact that the assumption of a quadratic variation in the response becomes less appropriate. Kaufman[14] *et al.* found that the accuracy of RS models for the wing weight in high dimensions can be increased by using conceptual level analyses to select an appropriate set of *intervening variables*.

Studies at Virginia Tech were performed using variable-complexity RS modeling techniques for both the aerodynamic design[7] and structural design[10,14] aspects of HSCT design. To this point, the aerodynamic design was performed using only panel level methods as the highest fidelity aerodynamic model instead of CFD solutions. The same is true for HSCT MDO performed by other groups at the Georgia Institute of Technology,[15,16] the University of Notre Dame,[17] and Stanford University.[18] Computer programs such as ACSYNT[19] and FLOPS[20] also perform aircraft MDO with lower fidelity aerodynamic and structural models.

Studies performed by Knill[21] *et al.* demonstrate significant changes in the HSCT performance estimates and aircraft weight resulting from the use of more accurate

Euler/Navier-Stokes aerodynamics in place of linear theory methods. The HSCT is a highly leveraged design, and its estimated performance is very sensitive to small changes in the predicted drag. An underprediction in the cruise drag of only 2 counts results in a 120 *n.mi.* overestimate of the range. The resulting aircraft TOGW is also sensitive to changes in the drag. A 2 count increase in the drag over the entire mission results in an increase in the optimal TOGW of $56,000$ *lb*. Clearly, more accurate aerodynamic predictions must be included in the design optimization. However, due to the large computational costs associated with complex CFD analyses, novel approaches must be devised to allow the implementation of high level calculations while retaining an efficient optimization procedure

A method has been developed which utilizes information gained from lower fidelity aerodynamic methods to more efficiently create response surface (RS) approximations to the supersonic Euler drag predictions. This method is tested using an existing multidisciplinary High-Speed Civil Transport (HSCT) design optimization procedure developed at Virginia Tech.[3–6] Conceptual level aerodynamic models provide the functional form of the drag polar:

$$C_D(\mathbf{x}) = C_{D_0}(\mathbf{x}) + K(\mathbf{x})\ {C_L}^2. \tag{1}$$

Response surface models of the *intervening functions*, $C_{D_0}(\mathbf{x})$ and $K(\mathbf{x})$, are created. Details of the RS modeling techniques are given in Appendix A. Response surface modeling techniques are employed using linear theory aerodynamic prediction methods to determine which terms in the RS models play a significant role in the evaluation of the drag. With this information, *reduced term* RS models representing a *correction* to the linear theory RS model predictions are constructed using fewer Euler evaluations. By eliminating unnecessary terms, the accuracy of the RS models is not compromised, and fewer CFD evaluations are required to evaluate the coefficients of the polynomials, thus reducing the problems associated with the curse of dimensionality. In addition, results from the inexpensive linear theory analyses are used to identify the suspected neighborhood of the optimal designs from Euler analyses. This enables smaller bounds on each design variables to be specified while maintaining confidence that the optimum lies within those bounds. This method is tested on simplified five, ten, fifteen, and twenty variable HSCT design problems.

2. HSCT Design Testbed

The design problem involves minimizing the take-off gross weight (TOGW) of a High-Speed Civil Transport (HSCT) with a 5500 *n.mi.* range. The aircraft is designed to cruise at Mach 2.4 and carry 250 passengers. The general HSCT configuration and mission is parameterized by 29 design variables. The aircraft geometry (Table 1) is described with 26 design variables. This provides a realistic description of the complex geometry with a relatively small number of design variables and allows the flexibility required to investigate a wide variety of aircraft configurations. Eight variables are used to describe the cranked delta planform (Fig. 2). The airfoil sections are described using five design variables. The axi-symmetric fuselage is defined with eight design variables which provide the fuselage radii at four axial *restraint* locations. The shape of the body between these points is then determined by considering it as a minimum wave drag body of a fixed volume.[4,22] The spanwise location of the nacelles is defined with two design variables. A single design variable describes the thrust of each engine. The horizontal and vertical tail areas are given by the final two geometric de-

Table 1: Twenty-Nine Variables in HSCT Design.

DV	Description
1	wing root chord, c_{root} (ft)
2	LE break, x (ft)
3	LE break, y (ft)
4	TE break, x (ft)
5	TE break, y (ft)
6	LE wing tip, x (ft)
7	wing tip chord, c_{tip} (ft)
8	wing semispan, $b/2$ (ft)
9	location airfoil max. thickness, $(x/c)_{max\text{-}t}$
10	LE radius parameter, R_{LE}
11	t/c at wing root, $(t/c)_{root}$
12	t/c at LE break, $(t/c)_{break}$
13	t/c at wing tip, $(t/c)_{tip}$
14	fuselage axial restraint #1, x_{fus_1} (ft)
15	fuselage radius at axial restraint #1, r_{fus_1} (ft)
16	fuselage axial restraint #2, x_{fus_2} (ft)
17	fuselage radius at axial restraint #2, r_{fus_2} (ft)
18	fuselage axial restraint #3, x_{fus_3} (ft)
19	fuselage radius at axial restraint #3, r_{fus_3} (ft)
20	fuselage axial restraint #4, x_{fus_4} (ft)
21	fuselage radius at axial restraint #4, r_{fus_4} (ft)
22	location of inboard nacelle, $y_{nacelle}$ (ft)
23	location of outboard nacelle (ft)
24	mission fuel weight, W_{fuel} (lb)
25	starting cruise altitude (ft)
26	cruise climb rate (ft/min)
27	vertical tail area (ft^2)
28	horizontal tail area (ft^2)
29	thrust per engine (lb)

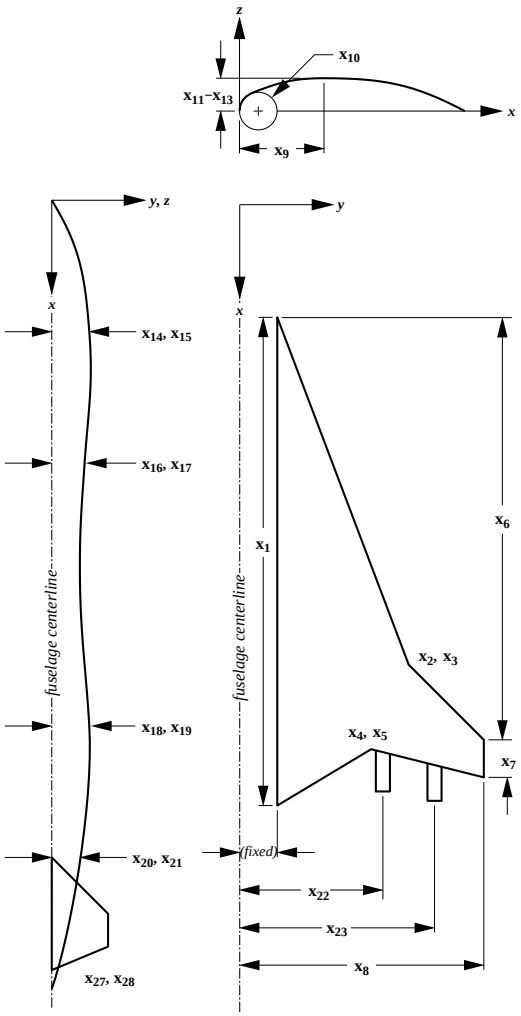

Figure 2: Geometry for 29-Variable HSCT Design Problem.

Table 2: Constraints in HSCT Design.

#	**Constraint Description**
1	Range $\geq 5,500\, n.mi.$
2	Required C_L at landing speed ≤ 1
3–20	Section $C_\ell \leq 2$
21	Landing angle of attack $\leq 12°$
22	Fuel volume $\leq$ half of wing volume
23	Spike prevention
24–41	Wing chord $\geq 7.0\, ft$
42–43	No engine scrape at landing α
44–45	No engine scrape at landing α, with 5° roll
46	No wing tip scrape at landing
47	Crosswind landing rudder deflection $\leq 22.5°$
48	Bank angle for crosswind landing $\leq 5°$
49	Takeoff rotation to occur ≤ 5 *sec*
50	Tail deflection for approach trim $\leq 22.5°$
51	Wing root T.E. $\leq$ horiz. tail L.E.
52	Balanced field length $\leq 11,000\, ft$
53	TE break scrape at landing with 5° roll
54	LE break $\leq$ semispan
55	TE break $\leq$ semispan
56–58	$(t/c)_{root}$, $(t/c)_{break}$, and $(t/c)_{tip} \geq 1.5\%$
59	$x_{fus_1} \geq 5ft$
60	$x_{fus_2} - x_{fus_1} \geq 10\, ft$
61	$x_{fus_3} - x_{fus_2} \geq 10\, ft$
62	$x_{fus_4} - x_{fus_3} \geq 10\, ft$
63	$300\, ft - x_{fus_4} \geq 10\, ft$
64	$y_{nacelle} \geq$ side of fuselage
65	$\Delta y_{nacelle} \geq 0$
66	Engine-out limit with vertical tail design; otherwise $y_{nacelle} + \Delta y_{nacelle} \leq 0.5(b/2)$
67-68	Maximum thrust required $\leq$ available thrust

sign variables. The idealized mission profile is composed of take-off, subsonic climb, supersonic cruise/climb, and landing segments. Three design variables describe the mission: the cruise climb rate, initial cruise altitude, and fuel weight.

A two-level optimization formulation is employed with the aerodynamic design as the upper level and the structural design as the lower level. The structural design takes the geometric information determined from the aerodynamic design and returns the structural weight. As described by Sobieszczanski-Sobieski and Haftka,[23] this asymmetric interaction between the two disciplines offers large savings in computational cost because there is no need to compute derivatives of the aerodynamic quantities with respect to the structural variables.

The aerodynamic design uses up to 68 inequality constraints (Table 2) dealing with the aircraft geometry and performance/aerodynamics. These constraints are devised to ensure feasible aircraft geometries and impose realistic performance and control capabilities. Fuel volume and wing chord length limits are examples of geometric constraints. Aerodynamic constraints include, for example, landing angle-of-attack limits; balanced field length requirements; and wing, tail, and engine scrape prevention criteria. Emergency conditions are used to enforce the landing constraints. It is assumed that the aircraft lands on a runway $5000\, ft$ above sea level at 145 *knots*, carrying 50% of its initial fuel weight. Other aerodynamic constraints establish controllability during adverse flight conditions. For example, the aircraft must be capable of trimmed flight with both engines on one side of the aircraft inoperable. These are complicated, nonlinear constraints that require aerodynamic forces and moments, stability

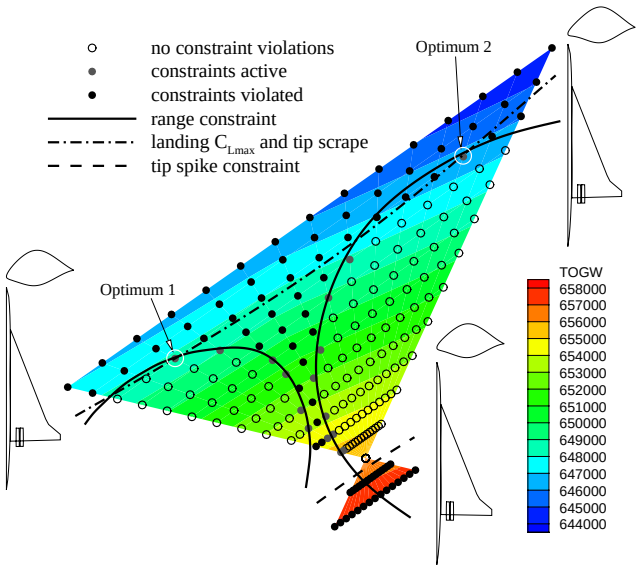

Figure 3: Nonconvex Design Space in Ten Variable Problem.

and control derivatives, and center of gravity and inertia estimates.

An example of the complicated constraint boundaries present in the design spaces associated with this HSCT optimization is shown in Fig. 3. This figure represents a plane in ten dimensional design space, created using three design points. Two of the design points represent local optima found by the optimizer, and the third point is a suboptimal feasible point. The remaining points on the plot are created by linearly varying all design variables between those three points. The design points represented by the open circles are feasible points, while those represented by the filled circles have violated some constraints. The plot clearly shows the nonconvexity of the design space caused by the aerodynamic constraints. If the optimizer drives the design near Optimum 1, it cannot cross the boundary created by the range constraint to arrive at Optimum 2 which is 2000 *lb* lighter. In addition to enabling the rapid creation of these types of useful plots, using response surface modeling techniques allows one to investigate a number of different starting points in the optimization in order to discover these local optima. The bulk of the computational effort is spent up front in the creation of the RS models, and performing a number of optimizations using the polynomial RS models is relatively inexpensive.

3. HSCT Design Tools

3.1. Linear Theory Aerodynamic Codes

The supersonic linear theory predictions are obtained from three codes, each computing a particular component of the drag. The volumetric wave drag is computed using the Harris[24] wave drag program. Drag-due-to lift is calculated using a panel method by Carlson[25] *et al.* with attainable leading edge thrust corrections.[26] Viscous drag estimates are obtained using standard algebraic estimates[27] of the skin friction.

The optimal camber for our HSCT designs is determined using the linear theory code WINGDES.[25,28] WINGDES attempts to find the camber distribution along the wing which minimizes the drag-due-to-lift. Two runs of WINGDES per wing were required to get the proper camber distribution. The second run serves to smooth the camber distribution and provide the maximum leading edge suction parameter closer to the design lift coefficient.

3.2. Computational Fluid Dynamics Code

Version 2.2 of the General Aerodynamic Simulation Program[29] (GASP) is used to obtain the Euler solutions. GASP is a fully conservative CFD code which solves the Reynolds averaged Navier-Stokes equations and many of its subsets. The code uses an upwind three dimensional finite volume spatial discretization. Roe, Van Leer, Steger-Warming, and full flux functions are available in each direction. For our calculations, a third order upwind biased interpolation of the Roe fluxes is used in each of the marching planes.

The finite volume formulation of the Reynolds averaged Navier-Stokes equations may be written in terms of the vector of conserved variables, Q, the vector of primitive variables, q, the cell volume, V, and a residual vector, $R(q)$, as

$$\frac{\partial <Q>}{\partial q}\frac{\partial <q>}{\partial t}V + R(q) = 0.$$

The cell averaged quantity, $<Q>$, is defined as an integral over the volume of the cell

$$<Q> = \frac{1}{V}\iiint_V Q(x,y,z,t)\,dV.$$

The cell averaged quantity for the primitive variables, $<q>$, is defined in the same manner. The residual vector can be written as a function of the cell edge area averages of the inviscid fluxes, $\vec{F}$ and viscous fluxes, $\vec{F_v}$, the unit normal vectors, $\hat{n}$, to the cell faces, and the areas, ΔA, of the nf cell faces as

$$R(q) = \sum_{j=1}^{nf}\left(\vec{F} - \vec{F_v}\right)\cdot\hat{n}_j\,\Delta A_j.$$

The norm of this residual vector represents the convergence to the steady state solution. GASP iteratively solves

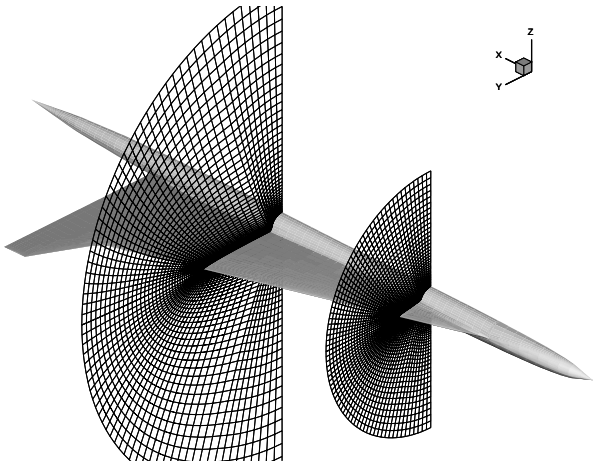

Figure 4: HSCT Wing-Fuselage with CFD Grid Planes.

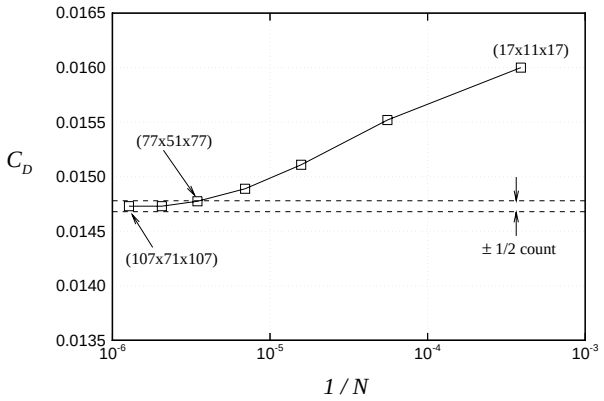

Figure 5: Euler Grid Convergence for Maneuver Wing.

the system of equations until a prescribed reduction in the residual norm is reached. Due to the large savings in computational time, space marching has been performed for all of the supersonic CFD calculations presented in this report.

3.3. Grid Generation

Grids suitable for space marching calculations on the HSCT wing-fuselage configurations are created using a grid generator originally developed by Barger.[30] The code has been modified by the author to provide better resolution of the leading edge and remain robust for large changes in the aircraft geometry. The grid generator receives as input the aircraft configuration stored in the Craidon[31] geometry format, extends the wing to join the fuselage, performs filleting of the wing-fuselage intersection,[32] and then creates a grid for space marching calculations. Since our HSCT optimization code creates a Craidon description file from its set of design variables, the conversion from a set of design variables to a space marching CFD grid is straightforward.

The space marching planes are created along planes of constant x-value. Two of these computational planes for a wing-fuselage configuration are shown in Fig. 4. A Mach cone analysis is used to form the outer boundary to ensure that all shocks are contained within the computational domain. The grid generator allows for flexible stretching of the grid points around and normal to the aircraft to create grids suitable for both Euler and Navier-Stokes calculations. Measures are employed to reduce grid skewness at the wing tip and wing-fuselage juncture. The grid generator is automated and robust for large planform changes, essential qualities for application in design optimization.

3.4. Code Validation

Verification of the CFD results has been performed to ensure solutions that are both grid and steady state converged. Figure 5 shows the convergence of the Euler drag coefficient with the number of grid cells, N, on a maneuver wing configuration. The accuracy of the CFD solutions has been ascertained through comparisons to experimental data of the forces and moments of forebody and wing geometries. Complete documentation of these studies are found in Ref. 21. These studies have confirmed that the Euler drag results are accurate within 1/2 count in the range of flight conditions considered.

3.5. Structural Analysis Codes

All components of the take-off gross weight are calculated using empirically based functions obtained from the Flight Optimization System[20] (FLOPS) weight equations. Work by Huang[33] *et al.* indicated that the FLOPS wing bending material weight predictions for HSCT configurations had insufficient accuracy. Substantial work has been performed using structural optimization from the finite element code GENESIS[34] to predict the wing bending material weight.[6,10,14] In this research, only the FLOPS weight equations are used in the HSCT optimization results.

3.6. Optimization Routine

Optimization is performed using Design Optimization Tools[35] (DOT). The constrained optimization is performed using sequential quadratic programming (SQP) and central difference gradient approximations.

4. Simplified HSCT Design Problems

A series of simplified optimization problems serve to evaluate the methods of including Euler analyses in multi-

Table 3: Active Design Variables in the Simplified Optimization Problems.

Design Variable	No. of Design Variables 5	10	15	20
Planform Variables				
c_{root}	X	X	X	X
c_{tip}	X	X	X	X
$b/2$		X	X	X
s_{LE_I}			X	X
Λ_{LE_I}	X	X	X	X
Λ_{LE_O}		X	X	X
s_{TE_I}	(straight TE)			X
Λ_{TE_I}	(straight TE)			X
Airfoil Variables				
$(x/c)_{max\text{-}t}$		X	X	X
R_{LE}		X	X	X
$(t/c)_{root}$	X	X	X	X
$(t/c)_{break}$	(t/c constant)			X
$(t/c)_{tip}$	(t/c constant)			X
Fuselage Variables				
x_{fus_1}				
r_{fus_1}			X	X
x_{fus_2}				
r_{fus_2}			X	X
x_{fus_3}				
r_{fus_3}			X	X
x_{fus_4}				
r_{fus_4}			X	X
Nacelle, Mission, and Empennage Variables				
$y_{nacelle}$		X	X	X
$\Delta y_{nacelle}$				X
W_{fuel}	X	X	X	X
Starting Cruise Alt.				
Cruise Climb Rate				
Vertical Tail Area				
Horizontal Tail Area	(No horizontal tail)			
Engine Thrust				

Table 4: Design Variable Limits in the Simplified Optimization Problems.

Design Variable	No. of Design Variables 5	10	15	20
Planform Variables				
c_{root}	$150 - 190\,ft$			
c_{tip}	$7 - 13\,ft$			
$b/2$	$[74\,ft]$	$58 - 78\,ft$		
s_{LE_I}	$[132\,ft]$		$105 - 135\,ft$	
Λ_{LE_I}	$67° - 76°$			
Λ_{LE_O}	$[25°]$	$12° - 32°$		
s_{TE_I}	(straight TE)			$10 - 30\,ft$
Λ_{TE_I}	(straight TE)			-55° – 16°
Airfoil Variables				
$(x/c)_{max\text{-}t}$	$[40\%]$	$38 - 52\%$		
R_{LE}	$[2.5]$	$2.1 - 4.1$		
$(t/c)_{root}$	$1.5 - 2.7\%$			
$(t/c)_{break}$	(t/c constant)			$1.5 - 2.7\%$
$(t/c)_{tip}$	(t/c constant)			$1.5 - 2.7\%$
Fuselage Variables				
x_{fus_1}	$[50\,ft]$			
r_{fus_1}	$[5.2\,ft]$	$4.5 - 6.0\,ft$		
x_{fus_2}	$[100\,ft]$			
r_{fus_2}	$[5.7\,ft]$	$4.5 - 6.0\,ft$		
x_{fus_3}	$[200\,ft]$			
r_{fus_3}	$[5.9\,ft]$	$4.5 - 6.0\,ft$		
x_{fus_4}	$[250\,ft]$			
r_{fus_4}	$[5.5\,ft]$	$4.5 - 6.0\,ft$		
Nacelle, Mission, and Empennage Variables				
$y_{nacelle}$	$[20\,ft]$	$10 - 35\,ft$		
$\Delta y_{nacelle}$	$[6\,ft]$			$6 - 18\,ft$
W_{fuel}	No Limits			
Starting Cruise Alt.	$[65,000\,ft]$			
Cruise Climb Rate	$[100\,ft/min]$			
Vertical Tail Area	$[548\,ft^2]$			
Horizontal Tail Area	(No horizontal tail)			
Engine Thrust	$[39,000\,lb]$			

$[\,\cdot\,]$ variable value when not active in the design

disciplinary HSCT design. The design variables (Table 3) used to define the geometry and mission are subsets of those used in the full 29 variable design, although some appear in a different form. For example, instead of specifying the x and y locations of the leading edge (LE) and trailing edge (TE) break points, the simplified problems use more meaningful variables specifying the wing sweep angles and the inboard surface lengths. In the same way, the variable specifying the x-location of the wing tip LE is replaced with a variable stipulating the outboard LE sweep angle. The upper and lower limits of the active design variables (Table 4) remain the same throughout the series of optimization problems. These bounds on the design variables are selected from optimization results performed using the linear theory RS models. These optima provided clues on the general location of the optimal designs from Euler analysis which allows smaller ranges on the design variables and results in more accurate RS model predictions.

The simplified designs are subject to a reduced set of constraints (Table 5). There are three basic reasons why certain constraints are eliminated:

1. The design variable(s) on which the constraints depend are not active.
2. Explicit limits on the design variables prevent geometric constraints from becoming active.
3. Simplifications to the mission eliminate related constraints.

Vertical tail sizing is not active for the simplified designs, therefore constraints number 47 and 48 do not appear. Unlike the 29 variable design, these configurations have no horizontal tail. This eliminates constraints 49, 50, and 51. The engine thrust also remains constant, removing constraints 52, 67, and 68 from the active list.

A simplified five variable wing design is considered first. The ten variable design problem is an extension of the five variable problem, enabling more general planform and airfoil geometries, and allowing variation in the spanwise location of the nacelles. Fuselage shaping is enabled with the fifteen variable design. Finally, the twenty variable design provides a complete description of the wing, airfoil, fuselage, and nacelles.

4.1. Five Variable HSCT Design

The geometry for the five variable wing design (Fig. 6) is created with four design variables specifying the root chord, c_{root}; tip chord, c_{tip}; inboard leading-edge (LE) sweep angle, Λ_{LE_I}; and the thickness-to-chord ratio, t/c. The fifth design variable gives the fuel weight, W_{fuel}. The allowable ranges of values for the variables are shown in Table 4. These ranges are chosen using results from previous optimization studies in an attempt to bracket the optimal designs within the bounds of the design variables. To uniquely describe the aircraft, a number of geometric parameters are specified. The fuselage and vertical tail shapes remain constant. The trailing edge (TE) for these configurations is straight with no TE break. The length of the LE from the wing apex to the LE break is constant ($s_{LE_I} = 132\,ft$), as is the sweep angle of the outboard LE ($\Lambda_{LE_O} = 25°$) and the wing semispan ($b/2 = 74\,ft$). Two airfoil parameters are held fixed: the leading-edge radius parameter ($R_{LE} = 2.5$) and the chordwise location of the maximum thickness ($(x/c)_{max\text{-}t} = 40\%$). The engine thrust, spanwise nacelle positions, relative position of the wing to the fuselage, and the cruise altitude are also invariant.

Table 5: Active Constraints in the Simplified Optimization Problems.

		No. of Variables			
#	**Constraint (Abbrev.)**	**5**	**10**	**15**	**20**
1	Range $\geq 5,500\,n.mi.$	X	X	X	X
2	C_L at landing speed	X	X	X	X
3–20	Section $C_\ell \leq 2$	X	X	X	X
21	Landing $\alpha \leq 12°$		X	X	X
22	Fuel volume	X	X	X	X
23	Spike prevention	X	X	X	X
24–41	Wing chord $\geq 7.0\,ft$	X	X	X	X
42–43	Engine scrape		X	X	X
44–45	Engine scrape (5° roll)		X	X	X
46	Wing tip scrape		X	X	X
47	Rudder deflection				
48	Bank angle $\leq 5°$				
49	Takeoff rotation				
50	Tail deflection				
51	Wing TE $\leq$ HT LE				
52	Balanced field length				
53	TE break scrape (5° roll)		X	X	X
54	LE break $\leq$ semispan	X	X	X	X
55	TE break $\leq$ semispan				X
56–58	$(t/c) \geq 1.5\%$				
59	$x_{fus_1} \geq 5ft$				
60	$x_{fus_2} - x_{fus_1} \geq 10\,ft$				
61	$x_{fus_3} - x_{fus_2} \geq 10\,ft$				
62	$x_{fus_4} - x_{fus_3} \geq 10\,ft$				
63	$300\,ft - x_{fus_4} \geq 10\,ft$				
64	$y_{nacelle} \geq$ fuselage				
65	$\Delta y_{nacelle} \geq 0$				
66	Engine-out limit; (vertical tail design)	X	X	X	X
67-68	Maximum thrust				
	Total Active Constraints	**42**	**49**	**49**	**50**

The optimization problem is the minimization of the take-off gross weight (TOGW) subject to 42 constraints (Table 5) related to both the geometry and the mission. Side constraints limit the values of the design variables. The optimization problem can be written as

$$\min_{\mathbf{x}\in\Re^5} TOGW\,(\mathbf{x})\,, \qquad (2)$$
$$\text{subject to: } \mathbf{g}(\mathbf{x}) \leq 0,$$
$$\mathbf{x_{min}} \leq \mathbf{x} \leq \mathbf{x_{max}}$$

where $\mathbf{x}$ is the five dimensional vector of design variables, and $\mathbf{g}(\mathbf{x})$ is the 42 dimensional vector of nonlinear inequality constraints. The minimum and maximum values of the

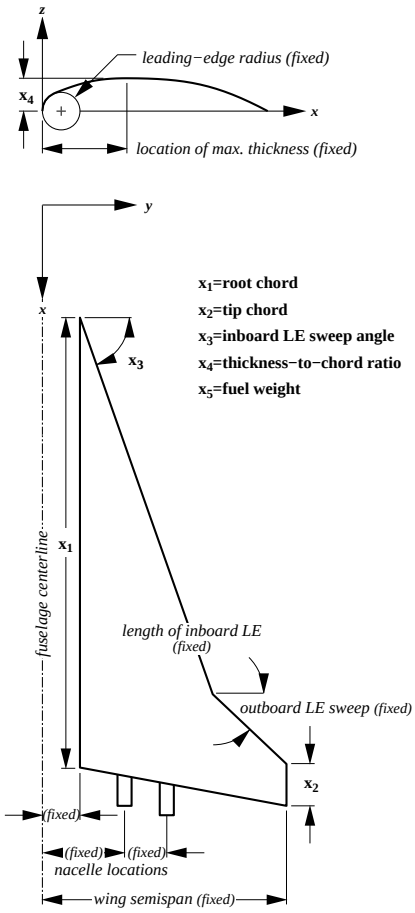

Figure 6: Geometry for Five Variable Design Problem.

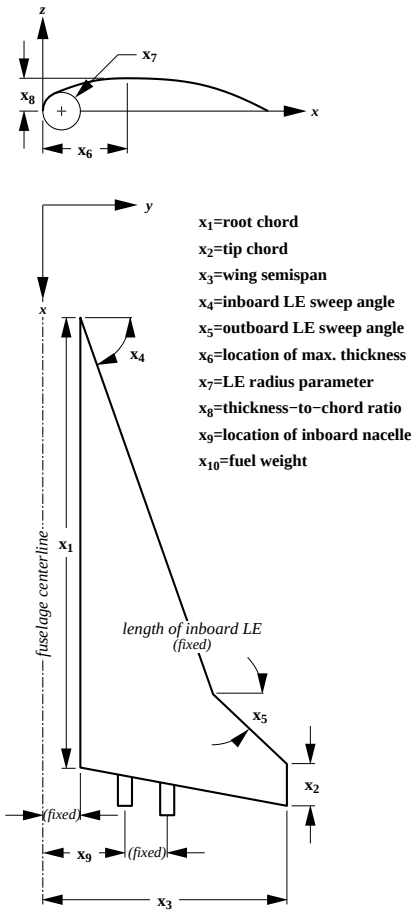

Figure 7: Geometry for Ten Variable Design Problem.

design variables are given by $\mathbf{x_{min}}$ and $\mathbf{x_{max}}$.

4.2. Ten Variable HSCT Design

The wing planform for the ten variable design (Fig. 7) is created with five design variables specifying the root chord, c_{root}; tip chord, c_{tip}; semispan, $b/2$; inboard LE sweep angle, Λ_{LE_I}; and outboard LE sweep angle, Λ_{LE_O}. The airfoil sections are described using three design variables: the leading-edge radius parameter, R_{LE}; location of maximum thickness, $(x/c)_{max\text{-}t}$; and thickness-to-chord ratio, t/c. The final two variables specify the inboard nacelle placement, $y_{nacelle}$, and the mission fuel weight, W_{fuel}. The allowable ranges of values for these variables are shown in Table 4. For these configurations, the fuselage and vertical tail shapes are fixed. The length of the leading edge from the wing apex to the leading-edge break is constant ($s_{LE_I} = 132\,ft$), and the trailing edge is straight. The engine thrust, spanwise distance between nacelles, relative position of the wing to the fuselage, and the cruise altitude are also fixed.

The optimization problem is to minimize the TOGW subject to 49 constraints (Table 5). This can be written as

$$\min_{\mathbf{x}\in\Re^{10}} TOGW\,(\mathbf{x})\,, \tag{3}$$
$$\text{subject to: } \mathbf{g}(\mathbf{x}) \leq 0,$$
$$\mathbf{x_{min}} \leq \mathbf{x} \leq \mathbf{x_{max}}$$

where $\mathbf{x}$ is the ten dimensional vector of design variables, and $\mathbf{g}(\mathbf{x})$ is the 49 dimensional vector of nonlinear inequality constraints.

4.3. Fifteen Variable HSCT Design

The wing planform for the fifteen variable design (Fig. 8) is created with six design variables specifying the root chord, c_{root}; tip chord, c_{tip}; semispan, $b/2$; inboard LE length, s_{LE_I}; inboard LE sweep angle, Λ_{LE_I}; and outboard LE sweep angle, Λ_{LE_O}. The airfoil sections are described using three design variables: the leading-edge radius parameter, R_{LE}; location of maximum thickness, $(x/c)_{max\text{-}t}$; and thickness-to-chord ratio, t/c. The fuselage radii, r_{fus_i},

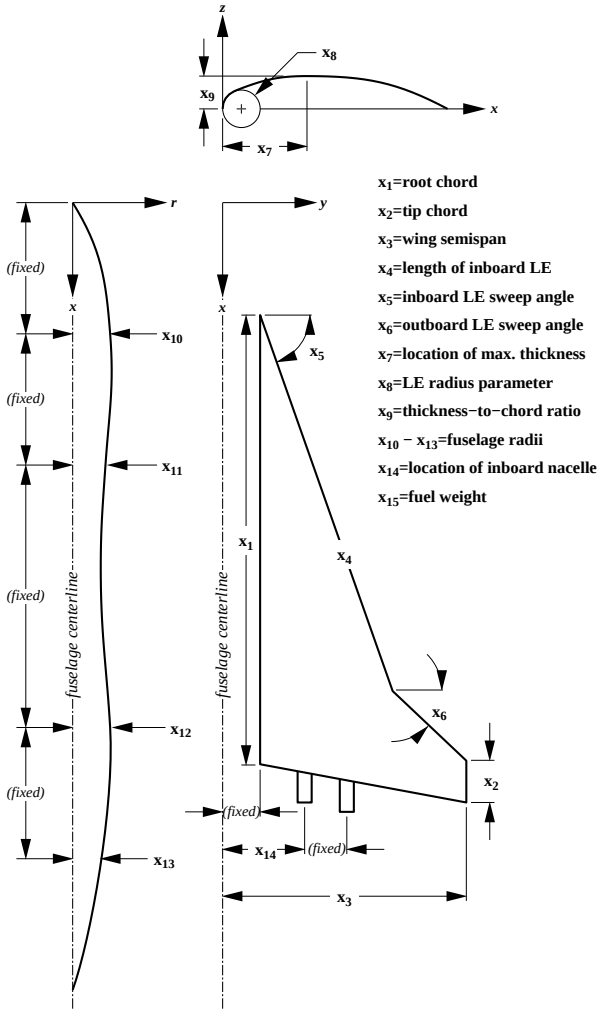

Figure 8: Geometry for Fifteen Variable Design Problem.

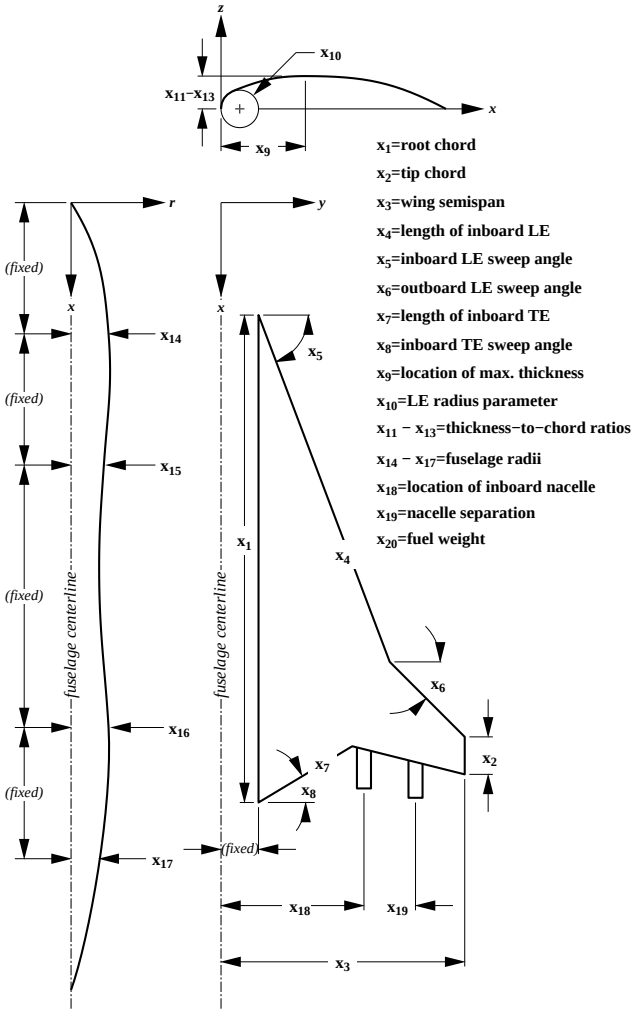

Figure 9: Geometry for Twenty Variable Design Problem.

are specified at four axial locations. The final variables specify the inboard nacelle placement, $y_{nacelle}$, and fuel weight, W_{fuel}. The allowable ranges of values for these variables are shown in Table 4. For these configurations, the wing TE is straight. The vertical tail shape, engine thrust, distance between nacelles, relative position of the wing to the fuselage, and the cruise altitude are constant.

The optimization problem is the minimization of the take-off gross weight (TOGW) subject to 49 constraints (Table 5) related to both the geometry and the mission. Side constraints limit the values of the design variables. The optimization problem can be written as

$$\min_{\mathbf{x}\in\Re^{15}} TOGW\,(\mathbf{x})\,, \tag{4}$$
$$\text{subject to: } \mathbf{g}(\mathbf{x}) \leq 0,$$
$$\mathbf{x_{min}} \leq \mathbf{x} \leq \mathbf{x_{max}}$$

where $\mathbf{x}$ is the fifteen dimensional vector of design variables, and $\mathbf{g}(\mathbf{x})$ is the 49 dimensional vector of nonlinear inequality constraints.

4.4. Twenty Variable HSCT Design

The wing planform for the twenty variable design (Fig. 9) is created with eight design variables specifying the root chord, c_{root}; tip chord, c_{tip}; semispan, $b/2$; inboard LE length, s_{LE_I}; inboard LE sweep angle, Λ_{LE_I}; outboard LE sweep angle, Λ_{LE_O}; the inboard TE length, s_{TE_I}; and the inboard TE sweep angle, Λ_{TE_I}. The airfoil sections are described using five design variables: the leading-edge radius parameter, R_{LE}; location of maximum thickness, $(x/c)_{max\text{-}t}$; and the thickness-to-chord ratios at the wing root, $(t/c)_{root}$, LE break, $(t/c)_{break}$, and wing tip, $(t/c)_{tip}$. The thickness-to-chord ratio is varied linearly between these three spanwise locations. The fuselage radii, r_{fus_i}, are

specified at four axial locations. The final variables specify the inboard nacelle placement, $y_{nacelle}$, the separation between the inboard and outboard nacelles, $\Delta y_{nacelle}$, and fuel weight, W_{fuel}. The allowable ranges of values for these variables are shown in Table 4. The vertical tail shape, engine thrust, relative position of the wing to the fuselage, and the cruise altitude are fixed.

The optimization problem is the minimization of the take-off gross weight (TOGW) subject to 50 constraints (Table 5) related to both the geometry and the mission. Side constraints limit the values of the design variables. The optimization problem can be written as

$$\min_{\mathbf{x}\in\Re^{20}} TOGW\left(\mathbf{x}\right), \tag{5}$$
$$\text{subject to: } \mathbf{g}(\mathbf{x}) \leq 0,$$
$$\mathbf{x_{min}} \leq \mathbf{x} \leq \mathbf{x_{max}}$$

where $\mathbf{x}$ is the twenty dimensional vector of design variables, and $\mathbf{g}(\mathbf{x})$ is the 50 dimensional vector of nonlinear inequality constraints.

5. Optimization Results

5.1. Five Variable HSCT Design

As discussed in Appendix A, using knowledge of the functional form of the drag polar eliminates the fuel weight dependency of the response. Therefore, response surface models for C_{D_0} and K are created using only four of the five design variables. The quadratic RS models therefore have $\frac{1}{2}\left(4+1\right)\left(4+2\right) = 15$ terms. A 3^{m-1} full factorial experimental design[36] is used for the initial screening of the four variable design space, giving a total of $3^4 = 81$ design points. None of these designs are geometrically infeasible, so the D-optimality criterion[37] is used to select the $2.0 \times n = 30$ design points to provide the computational experiments.

Results from stepwise regression analysis for the five variable design are shown in Fig. 10. The RMS error in the linear theory RS models represents the differences between the linear theory RS model prediction of the cruise drag and the linear theory analysis value. The RMS error in the incremental RS models represents the differences between the incremental RS model prediction of the cruise drag and the actual Euler value. These errors are computed at a 30 randomly selected set of design points at vertices of the design bounding box that are not used in the evaluation of the RS models. The regression analysis plot shows improved behavior in the errors for the incremental RS models as the number of terms is reduced. Recall that the incremental RS models are created by adding

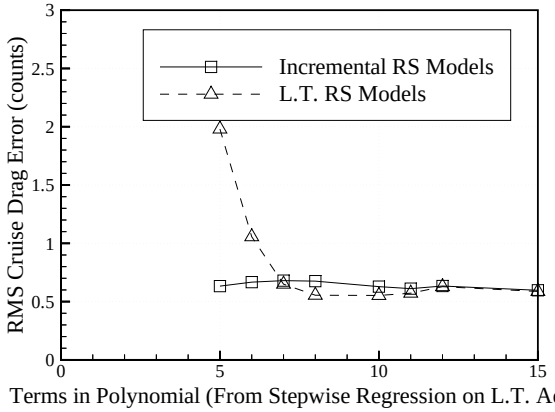

Figure 10: Stepwise Regression Analysis (5 Variable HSCT Design).

a reduced term correction RS models for the difference between the Euler and linear theory RS model predictions to the full term linear theory RS models. The RMS error in the cruise drag for the incremental RS models does not show the abrupt increase below seven terms that is present in the linear theory RS models.

The stepwise regression plot demonstrates two aspects that are vital to the success of the reduced term model approach. First, the stepwise regression technique is successful in eliminating unimportant terms from the response surface models. A large number of terms can be removed with little or no effect on the error. The second important aspect is that the errors in the reduced term incremental RS models, created using terms found from stepwise regression analysis on the linear theory RS models, do not change significantly as the number of terms is reduced. This indicates that linear theory analysis does reveal the terms that are important to the Euler analyses. In fact, it appears that the linear theory analysis presents a conservative estimate of the number of terms required for accurate Euler analysis.

The five term incremental RS model requires only 5.3 hours to create, as opposed to 16 hours required for the full term model. The optimal design obtained from the incremental RS models compares well (Fig. 11) to the full term Euler RS model. Even more importantly, Euler analysis on the optimal design reveals that the RS model cruise drag prediction is less than 1/10 count higher than the Euler value. The design variable values for the incremental RS model optimum fall within their prescribed bounds, demonstating the success of selecting these bounds based on the linear theory optimal designs. Table 6 shows that the corrected TOGW is only $700\,lb$ higher than that for

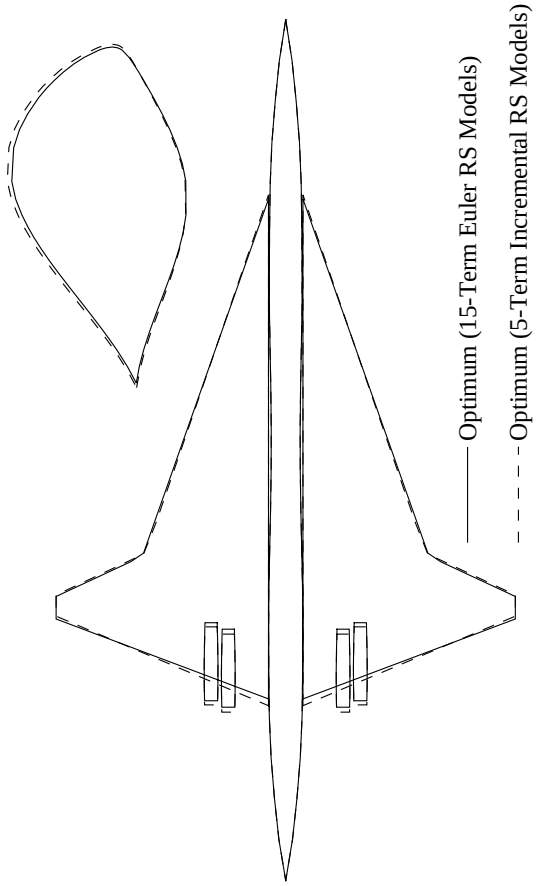

Figure 11: Optimal Designs from Reduced Term Incremental and Full Term Euler RS Models.

the full term Euler optimum. The corrected TOGW is the results of adding or subtracting fuel weight to the optimal designs in order to correct for the range discrepancy between the RS model and Euler predictions.

5.2. Ten Variable HSCT Design

Because of the lack of dependence on the fuel weight, the RS models for C_{D_0} and K are created using only nine of the ten design variables. The quadratic RS models therefore have $\frac{1}{2}(9+1)(9+2) = 55$ terms. A face centered central-composite experimental design[36] is used for the initial screening of the nine dimensional design space, giving a total of $2^9 + 2{\times}9 + 1 = 531$ design points. None of these designs are geometrically infeasible, so the D-optimality criterion is used to select the $2.5{\times}n = 138$ design points to provide the computational experiments.

Table 6: Optimal Design Variables (5 Variable HSCT Optimization).

	5 Term Incremental RS	**15 Term Euler RS**
c_{root}	$178.0\,ft$	$174.2\,ft$
c_{tip}	$7.4\,ft$	$7.8\,ft$
Λ_{LE_I}	$71.1°$	$70.6°$
t/c	1.81%	1.81%
W_{fuel}	$309,800\,lb$	$313,200\,lb$
W_{wing}	$103,900\,lb$	$103,900\,lb$
W_{TOGW}	$622,800\,lb$	$626,300\,lb$
Range: (Euler)	$5503\,n.mi.$	$5544\,n.mi.$
ΔW_{fuel}	$-320\,lb$	$-4010\,lb$
W_{C-TOGW}	$622,500\,lb$	$621,800\,lb$

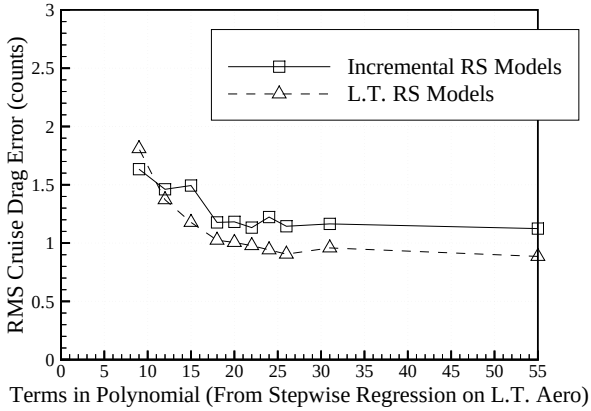

Figure 12: Stepwise Regression Analysis (10 Variable HSCT Design).

Stepwise regression analysis for the ten variable problem (Fig. 12) exhibits similar behavior of the incremental RS models as the number of terms is reduced. The RMS errors are computed at a 138 randomly selected set of the initial screening experimental design points that are not selected by the D-optimality criterion to create the RS models. As in the five variable problem, linear theory results capture the terms that are important to the Euler analyses. The optimal configuration is compared to the full term Euler RS models in Fig. 13, and the design variables are presented in Table 7. The RS model prediction of the cruise drag is 0.64 counts higher than the Euler value, leading to the $5542\,n.mi.$ actual range. Removing the extra fuel results in a design with no constraint violations that is $4000\,lb$ lighter than the full term Euler optimum.

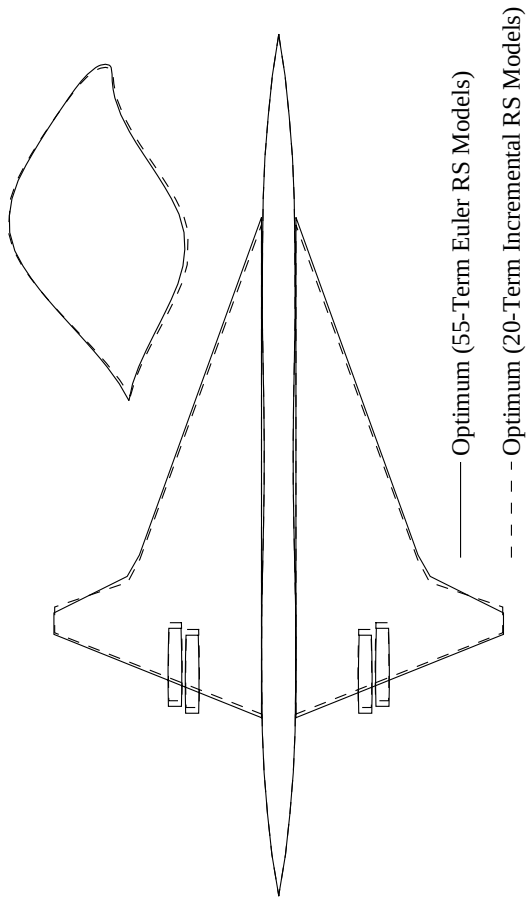

Figure 13: Optimal Designs from Reduced Term Incremental and Full Term Euler RS Models.

5.3. Fifteen Variable HSCT Design

For the fifteen-variable design, a central-composite experimental design[36] is used for the initial screening of the design space, giving a total of $2^{14} + 2{\times}14 + 1 = 16,413$ design points. The fuselage shaping results in 400 infeasible designs. For these designs, the fuselage radii and wing thickness are such that the wing root does not intersect the fuselage. The D-optimality criterion is used to select the $3.0{\times}n = 360$ out of the remaining $16,013$ design points to provide the computational experiments.

Stepwise regression analysis for the fifteen variable design is presented in Fig. 14. The RMS errors are computed at a 360 randomly selected set of the initial screening experimental design points that are not selected by the D-optimality criterion to create the RS models Optimization is performed with the 48 term incremental RS models. The

Table 7: Optimal Design Variables (10 Variable HSCT Optimization).

	20 Term Incremental RS	**55 Term Euler RS**
c_{root}	$170.4\,ft$	$174.3\,ft$
c_{tip}	$9.0\,ft$	$7.5\,ft$
$b/2$	$72.1\,ft$	$72.3\,ft$
Λ_{LE_I}	$70.0°$	$70.1°$
Λ_{LE_O}	$18.7°$	$26.5°$
$(x/c)_{max\text{-}t}$	50.2%	50.1%
R_{LE}	2.1	2.1
t/c	1.91%	1.82%
$y_{nacelle}$	$30.0\,ft$	$30.2\,ft$
W_{fuel}	$306,000\,lb$	$301,000\,lb$
W_{wing}	$96,100\,lb$	$99,200\,lb$
W_{TOGW}	$610,400\,lb$	$608,900\,lb$
Range: (Euler)	$5542\,n.mi.$	$5485\,n.mi.$
ΔW_{fuel}	$-3715\,lb$	$1300\,lb$
W_{C-TOGW}	$606,300\,lb$	$610,300\,lb$

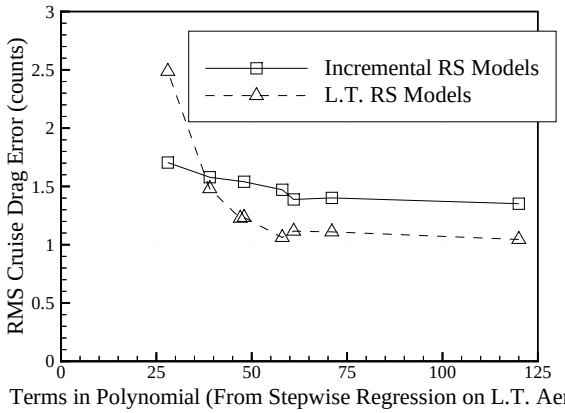

Figure 14: Stepwise Regression Analysis (15 Variable HSCT Design).

optimal designs from the full term Euler and reduced term incremental RS models (Fig. 15) are barely distinguishable from each other. Table 8 show the very close agreement in the design variables. In this region of the design space, both the Euler and incremental RS models are extremely accurate. This is evident in the fact that there is only a five mile discrepancy between the range estimates from the RS models and those from Euler evaluations. When the

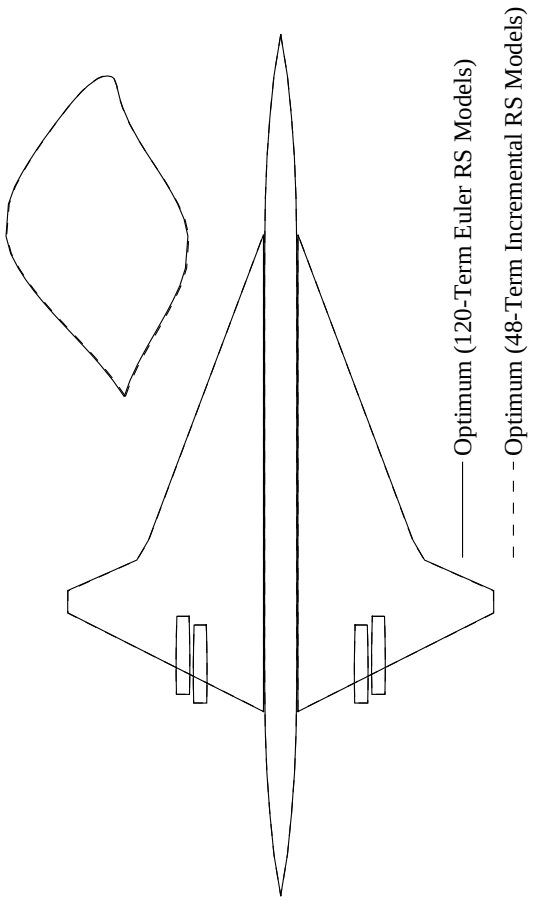

Figure 15: Optimal Designs from Reduced Term Incremental and Full Term Euler RS Models.

fuel weight is altered to counter the range variations, the TOGW for the Euler and incremental RS models are only 200 lb different.

5.4. Twenty Variable HSCT Design

A small-composite experimental design[36] is used for the initial screening of the twenty variable design space, giving a total of $2^{14} + 2{\times}19 + 1 = 16,423$ design points. From this set of configurations, 688 infeasible configurations are present. For some of these designs the fuselage radii and wing thickness are such that the wing root does not intersect the fuselage. Other infeasible designs had very small chord lengths near the wing LE break and negative taper ratios. The D-optimality criterion is used to select the $3.5{\times}n = 735$ out of the remaining $15,735$ design points to provide the computational experiments.

Table 8: Optimal Design Variables (15 Variable HSCT Optimization).

	48 Term Incremental RS	**120 Term Euler RS**
c_{root}	$166.2\,ft$	$166.2\,ft$
c_{tip}	$7.7\,ft$	$7.7\,ft$
$b/2$	$68.1°$	$68.2°$
s_{LE_I}	$120.4\,ft$	$120.3\,ft$
Λ_{LE_I}	$69.4°$	$69.4°$
Λ_{LE_O}	$24.2°$	$23.8°$
$(x/c)_{max\text{-}t}$	49.8%	49.7%
R_{LE}	2.1	2.1
t/c	1.99%	1.99%
r_{fus_1}	$5.2\,ft$	$5.1\,ft$
r_{fus_2}	$5.6\,ft$	$5.6\,ft$
r_{fus_3}	$5.6\,ft$	$5.6\,ft$
r_{fus_4}	$5.2\,ft$	$5.2\,ft$
$y_{nacelle}$	$28.1\,ft$	$28.0\,ft$
W_{fuel}	$299,614\,lb$	$300,100\,lb$
W_{wing}	$87,800\,lb$	$87,900\,lb$
W_{TOGW}	$590,700\,lb$	$591,500\,lb$
Range: (Euler)	$5495\,n.mi.$	$5505\,n.mi.$
ΔW_{fuel}	$450\,lb$	$-440\,lb$
W_{C-TOGW}	$\star 591,200\,lb$	$591,000\,lb$

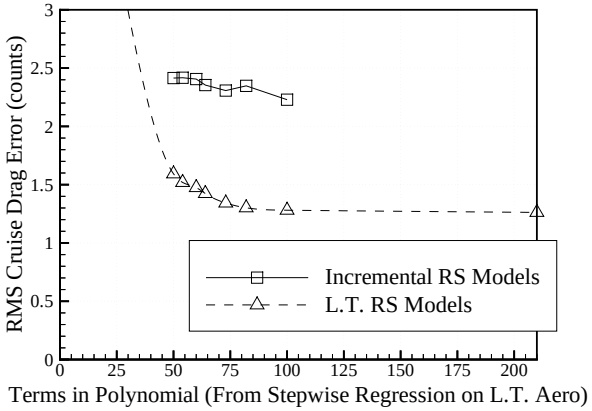

Figure 16: Stepwise Regression Analysis (20 Variable HSCT Design).

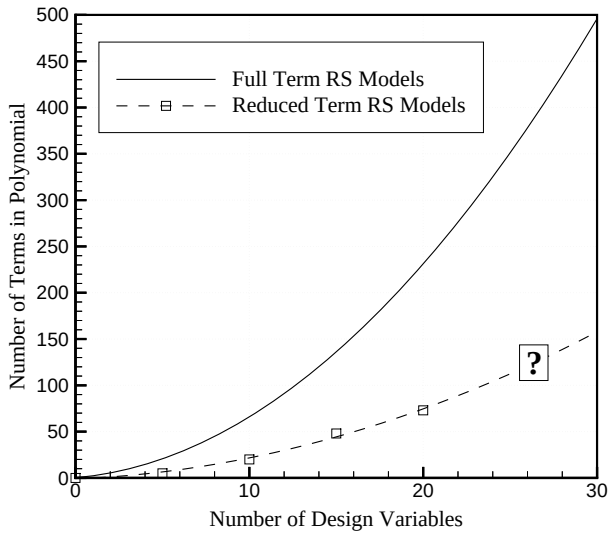

Figure 17: Terms in RS Models.

Due to computational expense, the full quadratic Euler RS models are not available for the twenty variable design. This is exactly the situation for which the reduced term incremental RS models were designed. Regression analysis on the linear theory data (Fig. 16) shows that the RMS cruise drag error remains nearly constant until about 73 terms remain in the RS models. A sufficient number of Euler evaluations were performed to create the 100 term incremental RS models. Since the full term Euler RS models are not present, this provides a model with which to evaluate the errors in the 73 term RS models. It is seen that there is no major difference in the cruise drag errors of the 100 term and 73 term incremental RS models. This is expected since the linear theory results have been conservative in selecting the number of terms in the RS models.

The optimal design from the incremental RS models is shown in Figure 18, and the optimal design variable values are presented in Table 9. The cruise drag prediction for the optimal design from the incremental RS models is 0.8 counts lower than the actual Euler value, which is much lower than the RMS error of the RS models. Compensating for the range deficiency gives a corrected TOGW of $588,000\,lb$. Although the error in the RS models is larger, this Euler optimum is $3000\,lb$ lighter than the 15 variable optimum.

Using the reduced term incremental RS models has provided a means to create RS models for high dimensional problems where computing the coefficients of the full quadratic RS models is not viable. Figure 17 shows how the present method extrapolates to 25 and 30 design variables. The trends indicate that a reduced term response surface model in 25 design variables can be created using the same number of terms as a full quadratic model in 15 design variables.

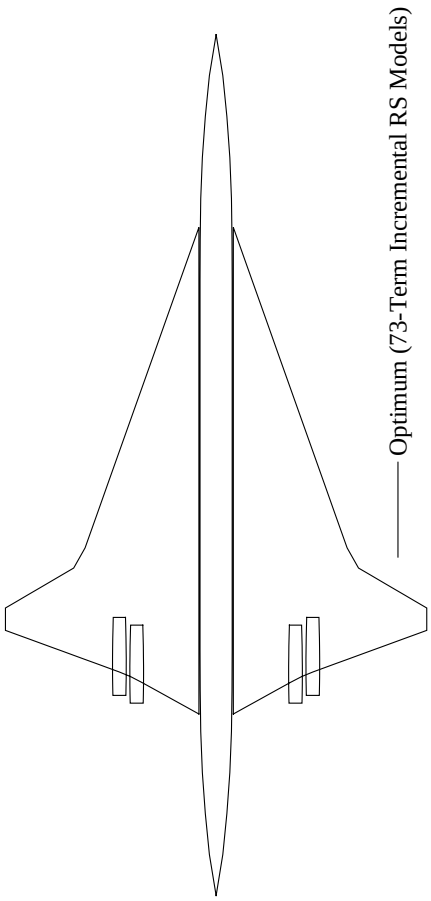

Figure 18: Optimal Design from Reduced Term Incremental RS Models.

5.5. RS Model Accuracy

The RMS errors in the incremental RS models are consistently higher than the errors in the optimal designs. Investigation led to the discovery that the incremental RS model fit through the interior of the design bounding box is better than that at the vertices. When evaluating the RMS error in the fifteen variable design using a new set of 162 design points scattered through the interior of the design box, the RMS error dropped from 1.5 counts to 0.9 count. This indicates that using points selected only from the vertices of the design box may not provide a sufficiently accurate representation of the RS model fit.

Table 9: Optimal Design Variables (20 Variable HSCT Optimization).

	73 Term Incremental RS
c_{root}	$169.5\,ft$
c_{tip}	$7.8\,ft$
$b/2$	$67.4\,ft$
s_{LE_I}	$124.8\,ft$
Λ_{LE_I}	$70.5°$
Λ_{LE_O}	$30.4°$
s_{TE_I}	$27.4\,ft$
Λ_{TE_I}	$-29.0°$
$(x/c)_{max\text{-}t}$	51.1%
R_{LE}	2.1
$(t/c)_{root}$	1.99%
$(t/c)_{break}$	1.91%
$(t/c)_{tip}$	1.94%
r_{fus_1}	$5.2\,ft$
r_{fus_2}	$5.6\,ft$
r_{fus_3}	$5.6\,ft$
r_{fus_4}	$5.2\,ft$
$y_{nacelle}$	$27.7\,ft$
$\Delta y_{nacelle}$	$6.0\,ft$
W_{fuel}	$293,000\,lb$
W_{wing}	$86,900\,lb$
W_{TOGW}	$583,200\,lb$
Range: (Euler)	$5449\,n.mi.$
ΔW_{fuel}	$4430\,lb$
W_{C-TOGW}	$\star 588,000\,lb$

$\star$ Adding fuel results in constraint violation

The RMS errors in the linear theory and incremental RS models steadily increase from satisfactory levels in the 5 variable to unacceptable levels in the 20 variable problem. Cursory examinations of three methods to improve the accuracy of the RS models have been investigated. The first method involves using a more accurate physical model to provide the functional form for the drag polar. With an additional CFD evaluation per design, a more accurate cambered form of the drag polar, $C_D(\mathbf{x}) = C_{D_m}(\mathbf{x}) + K(\mathbf{x})\ [C_L - C_{L_m}(\mathbf{x})]^2$, can be evaluated. While not addressing the nonquadratic behavior of the response, this approach was found to reduce the RMS error in the RS models by approximately 0.3 count. The nonquadratic nature of the response can be addressed in two ways: reducing the size of the design bounding box and including cubic terms in the RS model. Reducing the size of the design box has a significant effect on the error; however, care must be taken to ensure that the optimal design lies within the reduced box. Including cubic terms allows one to maintain the size of the original box, but the computational expense of evaluating all the cubic terms makes it unattractive for high dimensional problems. Using the more accurate drag polar along with a "zooming" technique to reduce the size of the design box appears to be a promising approach.

6. Conclusions

A method for efficiently implementing supersonic Euler analyses in a combined aerodynamic–structural optimization of a HSCT configuration has been developed and tested on problems of five, ten, fifteen, and twenty design variables. This method takes advantage of information obtained from inexpensive lower fidelity aerodynamic analyses to more effectively create RS models for the Euler solutions. Accuracy of the RS model predictions is enhanced by selecting the functional form of the drag polar, $C_D = C_{D_0}(\mathbf{x}) + K(\mathbf{x})\ {C_L}^2$, based on conceptual level aerodynamic models and creating RS models involving the *intervening functions* $C_{D_0}(\mathbf{x})$ and $K(\mathbf{x})$. Creating *correction* RS models representing the difference between linear theory and Euler values of the intervening functions, $\Delta C_{D_0}(\mathbf{x})$ and $\Delta K(\mathbf{x})$, proves advantageous. *Incremental* RS models for the Euler predictions are then created by adding the correction RS models to the quadratic linear theory RS models. Optimization results from the linear theory RS models are used to select the design bounding box within which the optimum from Euler analysis should lie. This improves the accuracy of the RS models by allowing smaller ranges on the design variables compared to those required if no information was available on the general location of the optimal design. Errors in the RS model cruise drag predictions, based on actual Euler calculations, for the optimal designs range from 0.1 counts to 0.8 counts for the twenty variable optimum.

Computational expense is reduced using stepwise regression analysis results gained from linear theory analysis. Stepwise regression analysis removes terms from the quadratic polynomial RS models that are not important in the evaluation of the response. Since the Mach 2.4 cruise flight regime is predominantly linear, terms that are unimportant to the linear theory RS models are also unimportant to Euler RS models. By removing unnecessary terms, the number of CFD analyses required to evaluate the co-

efficients in the resulting *reduced term* RS models, and therefore the computational effort, is reduced. Creating the reduced term RS models results in a savings of 11 hours, 47 hours, 115 hours, and 255 hours of CPU time on a single 75 MHz IP21 processor of a SGI *Power Challenge* for the five, ten, fifteen, and twenty variable design problems, respectively. For consistency all times are given in terms of single processor performance, however parallel computing is performed on the 119 node, distributed memory Intel *Paragon* XP/S at Virginia Tech to reduce the computational burden.

The bulk of the computational effort involved in using the RS approach to optimization lies in the initial creation of the RS models. After they are created, the RS models can be evaluated and used repeatedly with minimal computational effort. This is exploited by using more accurate central difference gradient information in the optimization, which would be very expensive in high dimensional problems without the use of RS models. In addition, valuable information concerning the complex design spaces encountered and design trade-offs and sensitivities can be obtained through the simple evaluation of a polynomial.

While the cruise drag errors in the optimal designs are within 1 count, the RMS errors in the RS models steadily increase from the five through the twenty variable problems. The inability to perform calculations at all vertices of the design bounding box and the nonquadratic behavior of the response are contributing factors. These errors can be reduced by using the more accurate functional form of the drag polar, $C_D(\mathbf{x}) = C_{D_m}(\mathbf{x}) + K(\mathbf{x})\ [C_L - C_{L_m}(\mathbf{x})]^2$. However, other methods are necessary to bring the RS model errors in the twenty variable case to acceptable levels. Using the more accurate drag polar along with a "zooming" technique to reduce the size of the design box appears to be a promising approach. Research is currently under way to investigate the use of these procedures in the multidisciplinary HSCT design problem.

Acknowledgments

Support for this research effort was provided through the NASA Langley Research Center grants NAG1–1160 with Mr. Peter Coen as contract monitor and NAG1–1562 with Dr. Perry Newman as contract monitor.

References

[1] J. P. Geising, S. Agrawal, and B. K. Bharadvaj. "The Role of Computational Fluid Dynamics in Multidisciplinary Design Optimization of Transport Aircraft," *Proceedings of the Sixth International Symposium on Computational Fluid Dynamics, Technology, and Operations Congress*, Lake Tahoe, CA, September 4–7, 1995.

[2] L. M. Nicolai. *Fundamentals of Aircraft Design*, E.P. Domicone Printing Services, Fairborne, OH, pp. 24-23–24-25, 1975.

[3] M. G. Hutchison, E. R. Unger, W. H. Mason, B. Grossman, and R. T. Haftka. "Aerodynamic Optimization of an HSCT Configuration Using Variable-Complexity Modeling," AIAA Paper No. 93–0101, January 1993.

[4] M. G. Hutchison, E. R. Unger, W. H. Mason, B. Grossman, and R. T. Haftka. "Variable-Complexity Aerodynamic Optimization of a High-Speed Civil Transport Wing," *Journal of Aircraft*, 31, No. 1: 110–116, 1994.

[5] J. Dudley, X. Huang, R. T. Haftka, B. Grossman, and W. H. Mason. "Variable-Complexity Interlacing of Weight Equation and Structural Optimization of the High-Speed Civil Transport," AIAA Paper No. 94–4377, September 1994.

[6] J. Dudley, X. Huang, P. E. MacMillin, B. Grossman, R. T. Haftka, and W. H. Mason. "Multidisciplinary Optimization of the High-Speed Civil Transport," AIAA Paper No. 95–0124, January 1995.

[7] A. A. Giunta, V. Balabanov, D. Haim, B. Grossman, W. H. Mason, L. T. Watson, and R. T. Haftka. "Wing Design for a High-Speed Civil Transport Using a Design of Experiments Methodology," *Proceedings of the Sixth AIAA/NASA/ISSMO Symposium on Multidisciplinary Analysis and Optimization,* AIAA Paper No. 96–4001, pp. 168–183, Bellevue, WA, September 1996.

[8] G. Venter, R. T. Haftka, and J. H. Starnes. "Construction of Response Surfaces for Design Optimization Applications," *Proceedings of the Sixth AIAA/NASA/ISSMO Symposium on Multidisciplinary Analysis and Optimization,* AIAA Paper No. 96–4040, pp. 548–564, Bellevue, WA, September 1996.

[9] A. A. Giunta, R. Narducci, S. Burgee, B. Grossman, W. H. Mason, L. T. Watson, and R. T. Haftka. "Variable-Complexity Response Surface Aerodynamic Design of an HSCT Wing," *Proceedings of the Thirteenth AIAA Applied Aerodynamics Conference,*AIAA Paper No. 95–1886, pp. 994–1002, San Diego, CA, June 1995.

[10] V. Balabanov, M. Kaufman, D. L. Knill, D. Haim, O. Golovidov, A. A. Giunta, R. T. Haftka, B. Grossman, W. H. Mason, and L. T. Watson. "Dependence of Optimal Structural Weight on Aerodynamic Shape for a High-Speed Civil Transport," *Proceedings of the Sixth AIAA/NASA/ISSMO Symposium on Multidisciplinary Analysis and Optimization,* AIAA Paper No. 96–4046, pp. 599–612, Bellevue, WA, September 1996.

[11] V. O. Balabanov. *Development of Approximations for HSCT Wing Bending Material Weight Using Response Surface Methodology*, Ph.D. thesis, Department of Aerospace and Ocean Engineering, Virginia Polytechnic Institute and State University, 1997.

[12] R. S. Sellar, M. A. Stelmack, S. M. Batill, and J. E. Renaud. "Response Surface Approximations for Discipline Coordination in Multidisciplinary Design Optimization," *Thirty-seventh AIAA/ASME/ASCE/AHS/ASC Sructures, Structural Dynamics, and Materials Conference,* AIAA Paper No. 96–1383, Salt Lake City, UT, April 1996.

[13] W. Chen, J. K. Allen, D. P. Schrage, and F. Mistree. "Statistical Experimentation Methods for Achieving Affordable Concurrent Systems Design," *AIAA Journal*, 35, No. 5, May 1997.

[14] M. Kaufman, V. Balabanov, S. L. Burgee, A. A. Giunta, B. Grossman, W. H. Mason, L. T. Watson, and R. T. Haftka. "Variable-Complexity Response Surface Approximations for Wing Structural Weight in HSCT Design," AIAA Paper No. 96–0089, January 1996.

[15] D. A. DeLaurentis, C. E. Cesnik, J.-M. Lee, D. N. Mavris, and D. P. Schrage. "A New Approach to Integrated Wing Design in Conceptual Synthesis and Optimization," *Proceedings of the Sixth AIAA/NASA/ISSMO Symposium on Multidisciplinary Analysis and Optimization,* AIAA Paper No. 96–4000, pp. 1835–1843, Bellevue, WA, September 1996.

[16] P. J. Röhl, D. N. Mavris, and D. P. Schrage. "Combined Aerodynamic and Structural Optimization of a High-Speed Civil Transport," *Thirty-sixth AIAA Structures, Dynamics, and Materials Conference,* AIAA Paper No. 95-1222, New Orleans, LA, April 1995.

[17] R. S. Sellar, S. M. Batill, and J. E. Renaud. "Response Surface Based, Concurrent Subspace Optimization for Multidisciplinary System Design," *Thirty-fourth Aerospace Sciences Meeting and Exhibit,* AIAA Paper No. 96–0714, 1996.

[18] I. Kroo, S. Altus, R. Braun, P. Cage, and I. Sobieski. "Multidisciplinary Methods for Aircraft Preliminary Design," *Proceedings of the Fifth AIAA/USAF/NASA/ISSMO Symposium on Multidisciplinary Analysis and Optimization,* AIAA Paper No. 94-4325, pp. 697–707, Panama City, FL, September 1994.

[19] S. Jayaram, A. Myklebust, and P. Gelhausen. "ACSYNT—A Standards-Based System for Parametric Computer Aided Conceptual Design of Aircraft," AIAA Paper No. 92-1268, 1992.

[20] L. A. McCullers. "Aircraft Configuration Optimization Including Optimized Flight Profiles," *Proceedings of Symposium on Recent Experiences in Multidisciplineary Analysis and Optimization,* J. Sobieski, compiler, NASA CP–2327, pp. 396–412, April 1984.

[21] D. L. Knill, V. Balabanov, O. Golovidov, B. Grossman, W. H. Mason, R. T. Haftka, and L. T. Watson. "Accuracy of Aerodynamic Predictions and Its Effects on Supersonic Transport Design," *MAD Center Report 96–12–01*, Multidisciplinary Analysis and Design Center for Advanced Vehicles, Virginia Tech, Blacksburg, VA, December 1996.

[22] E. Eminton. "On the Minimization and Numerical Evaluation of Wave Drag," *Royal Aircraft Establishment Report AERO.2564*, November 1955.

[23] J. Sobieszczanski-Sobieski and R. T. Haftka. "Multidisciplinary Aerospace Design Optimization: Survey of Recent Developments," *Thirty-fourth Aerospace Sciences Meeting and Exhibit,* AIAA Paper No. 96–0711, Reno, NV, January 15–18, 1996.

[24] R. V. Harris, Jr. "An Analysis and Correlation of Aircraft Wave Drag," NASA TM X–947, 1964.

[25] H. W. Carlson and D. S. Miller. "Numerical Methods for the Design and Analysis of Wings at Supersonic Speeds," NASA TN D–7713, 1974.

[26] H. W. Carlson and R. J. Mack. "Estimation of Leading-Edge Thrust for Supersonic Wings of Arbitrary Planforms," NASA TP–1270, 1978.

[27] E. J. Hopkins and M. Inouye. "An Evaluation of Theories Predicting Turbulent Skin Friction and Heat Transfer on Flat Plates at Supersonic and Hypersonic Mach Numbers," *AIAA Journal*, 9, No. 6: 993–1003, June 1971.

[28] H. W. Carlson and K. B. Walkley. "Numerical Methods and a Computer Program for Subsonic and Supersonic Aerodynamic Design and Analysis of Wings with Attainable Thrust Corrections," NASA CR–3808, 1984.

[29] W. D. McGrory, D. C. Slack, M. P. Applebaum, and R. W. Walters. *GASP Version 2.2 Users Manual*, Aerosoft, Inc., Blacksburg, VA, 1993.

[30] R. L. Barger, M. S. Adams, and R. R. Krishnan. "Automatic Computation of Euler-Marching and Subsonic Grids for Wing-Fuselage Configurations," NASA TM 4573, July 1994.

[31] C. B. Craidon. "Description of a Digital Computer Program for Airplane Configuration Plots," NASA TM X–2074, 1970.

[32] R. L. Barger and M. S. Adams. "Automatic Computation of Wing-Fuselage Intersection Lines and Fillet Inserts with Fixed-Area Constraint," NASA TM 4406, March 1993.

[33] X. Huang, R. T. Haftka, B. Grossman, and W. H. Mason. "Comparison of Statistical Weight Equations with Structural Optimization for Supersonic Transport Wings," AIAA Paper No. 94–4379, September 1994.

[34] Vanderplaats, Miura and Associates, Inc. *GENESIS User Manual, Version 1.3*, 5960 Mandarin Avenue, Suite F, Goleta, CA 93117, 1993.

[35] Vanderplaats Research & Development, Inc. *DOT Users Manual, Version 4.20*, Colorado Springs, CO, 1995.

[36] R. Mead. *The Design of Experiments*, Cambridge University Press, New York, NY, pp. 542–548, 1988.

[37] M. J. Box and N. R. Draper. "Factorial Designs, the $|\mathbf{X}^T\mathbf{X}|$ Criterion, and Some Related Matters," *Technometrics*, 13, No. 4, pp. 731–742, 1971.

[38] R. H. Myers and D. C. Montgomery. *Response Surface Methodology: Process and Product Optimization Using Designed Experiments*, John Wiley & Sons, Inc., New York, NY, pp. 1–67, 134–174, 297–357, 640–655, 1995.

[39] SAS Institute, Inc. *JMP Users Guide, Version 3.1*, Cary, NC, 1995.

[40] T. J. Mitchell. "An Algorithm for the Construction of D-Optimal Experimental Designs," *Technometrics*, 16, No. 2, pp. 203–210, 1974.

[41] M. D. Kaufman. *Variable-Complexity Response Surface Approximations for Wing Structural Weight in HSCT Design*, Master's thesis, Department of Aerospace and Ocean Engineering, Virginia Polytechnic Institute and State University, 1996.

[42] O. B. Golovidov. *Variable-Complexity Response Surface Approximations for Aerodynamic Parameters in HSCT Design*, Master's thesis, Department of Aerospace and Ocean Engineering, Virginia Polytechnic Institute and State University, 1997.

[43] A. A. Giunta, J. M. Dudley, R. Narducci, B. Grossman, R. T. Haftka, W. H. Mason, and L. T. Watson. "Noisy Aerodynamic Response and Smooth Approximations in HSCT Design," *Proceedings of the Fifth AIAA/USAF/NASA/ISSMO Symposium on Multidisciplinary Analysis and Optimization,* AIAA Paper No. 94-4376, pp. 1117–1128, Panama City, FL, September 1994.

A. Response Surface Modeling

To use relatively expensive Euler solutions for the large number of constraint evaluations required in our multidisciplinary optimization, RS models of the supersonic aerodynamics are created. Response surface modeling techniques for aerodynamic and structural design improve the performance of highly constrained gradient based optimizations.[7,10,12,13] Using RS models offers a number of benefits. First, the RS models smooth out numerical noise present in the analyses. This noise can distort gradient information and lead to artificial local minima in the design space. Second, the analysis codes are separated from the optimization routines. This eliminates problems associated with integrating large, production level grid generators, analysis codes, and post processing utilities. It also allows analyses to be performed by experts in the specific discipline on parallel architecture machines. Results from parallel computing efforts are described in Section B. Finally, by replacing complex analysis codes with simple quadratic polynomials, one can readily obtain information on design trade-offs, sensitivities to certain variables, and insight into the highly constrained, nonconvex design spaces. These aspects are presented in Appendix C.

A.1. Design of Experiments

Design of experiments (DOE) theory provides a systematic means of selecting the set of points (called an *experimental design*) within the design space at which to perform computational analyses. The 2^m vertices formed by the upper and lower bounds on the design variables define the *design bounding box* or *hypercube* within which the

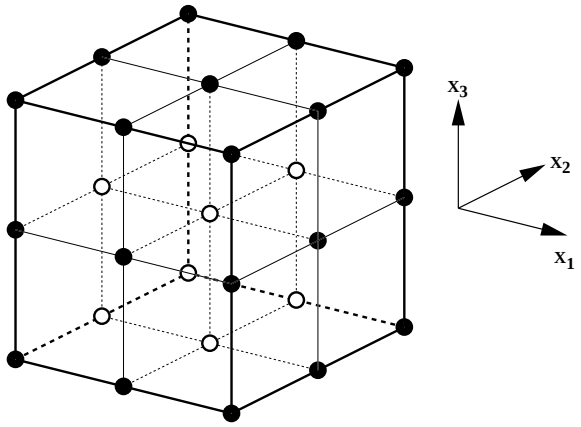

Figure 19: 3^3 Full Factorial Experimental Design.

experimental design is created. The range of each design variable is scaled to span $[-1, 1]$ for both numerical stability and ease of notation.[38] To create the experimental design, the ranges of the design variables are discretized at evenly spaced intervals. For example, a 2^m full factorial design is created by specifying each design variable at two levels: the lower bound (-1) and the upper bound (1). Therefore, this experimental design consists of every vertex in the design bounding box. The type of experimental design created is defined by the number of intervals and the distribution of the points on those intervals. The choice of experimental design depends on the dimension of the problem, the computational resources available, and the type of function to which one wishes to fit the data. Four types of experimental designs are used in this research: 3^m *full factorial experimental designs*,[36] *face centered central-composite designs*,[36,38] *small-composite designs*,[38] and *D-optimal experimental designs*.[37]

A 3^m full factorial design[36] is created by specifying the design variables at three levels (−1,0,1) corresponding to the lower bound, midpoint, and upper bound of the design variables. A 3^3 experimental design is presented in Fig. 19. This experimental design provides sufficient information to construct quadratic polynomial RS models. However, as the number of design variables increases, the number of computational experiments required becomes prohibitively large. For example, a 3^m full factorial design in twenty dimensional space requires $3^{20} \approx 3.5{\times}10^9$ computational experiments.

A face centered central-composite design[36,38] (CCD) enables resolution of quadratic terms in the RS models with fewer computational experiments. It is created by taking a 2^m full factorial design and adding $2m$ "star" points on the faces of the hypercube and another point in the middle of the design hypercube. The "star" points correspond to a set of design variables in which all variables are held at their midpoint value except for a single variable which is specified at either its upper or lower bound. As the number of design variables is further increased, these experimental designs also become prohibitively large. Creating a face centered CCD in a twenty dimensional space requires $2^{20} + 2 \cdot 20 + 1 \approx 1.0{\times}10^6$ computational experiments.

The small-composite experimental design[38] allows even fewer computational experiments with which to evaluate quadratic RS models. This experimental design is constructed in a manner similar to that for the central-composite design except that a *fractional factorial*[38] experimental design is used in place of the 2^m full factorial design. The fractional factorial design includes only $2^{m-\beta}$ vertices of the m dimensional bounding box (β is an integer number smaller than m). There is some freedom in the value of β, however it can not be too large or there will be insufficient data to properly resolve all terms in the quadratic polynomial. Certain vertices of the design space will not have any associated data when using this experimental design. While this is not an ideal situation, it is inevitable since the number of vertices grows exponentially with the number of design variables.

The final experimental design used in this study is the D-optimal experimental design.[37] D-optimal designs allow great flexibility in the number of computational experiments that is not allowed in the previously discussed experimental designs. D-optimal designs are also well suited for irregularly shaped design spaces, while the classical designs are geared toward rectangular design spaces. D-optimal designs minimize the uncertainty in the polynomial coefficient estimates and in the predicted value of the response. To create a D-optimal experimental design, one selects p design points out of q candidate points. In this research, the candidate points are derived from one of the three classical experimental designs described above. An iterative optimization method is then used to find the p D-optimal points.

For the five and ten variable cases, the JMP[39] statistical software package is used to provide the D-optimal designs. The approach implemented in JMP uses sets of randomly selected seed candidate points, and the best points in terms of the prediction variance are kept throughout the iterative procedure. Because the design points are selected in a quasi-random manner, it is unlikely that the experimental design chosen from JMP is truly a D-optimal set. Limitations in JMP prevent its use for the larger design problems. A routine employing Mitchell's "k-exchange" method,[40] developed by Dr. Dan Haim, is used for the fifteen and twenty variable cases.

A.2. Functional Form of the Response

Conceptual level aerodynamic models provide useful information into basic relationships between the lift and drag coefficients. One of the simplest relationships is the uncambered form of the drag polar, which is written as

$$C_D(\mathbf{x}) = C_{D_0}(\mathbf{x}) + K(\mathbf{x})\ {C_L}^2. \tag{6}$$

Knowledge of the functional form of the aircraft drag suggests using RS models for the intervening functions, C_{D_0} and K, instead of a single RS model for the drag coefficient, C_D, itself. There are a number of reasons why this approach is beneficial:

1. C_{D_0} and K are functions of only the geometric variables, thereby reducing the dimension of the RS model by eliminating mission related variables such as the fuel weight. The fuel weight is represented completely by C_L.

2. From a design standpoint, more insight is obtained from the intervening functions than from individual drag values.

3. Using knowledge of the simple aerodynamic theory enables the selection of an accurate functional form for the response without relying on the RS models to capture the correct form. In the same way, Kaufman[41] used information about the basic form of statistical weight functions to improve the accuracy of RS models for the wing bending material weight.

4. Experience has indicated that more accurate results are obtained by building the function from quadratic RS models for its components, instead of using a single RS model for C_D. Golovidov[42] found similar improvements in the accuracy of the aircraft range predictions by using RS models for the drag components to compute the range rather than using RS models for the range itself.

The HSCT wings have little camber since they are optimized for cruise at Mach 2.4; therefore, this form of the drag polar for uncambered wings is still fairly accurate. The error in fitting the Euler drag polars to this form is less than 0.5 count over $0.05 \leq C_L \leq 0.12$. These values of C_L cover the range of cruise lift coefficients found for our HSCT designs.

A.3. Creating Quadratic RS Models

The procedure for creating the RS models for C_{D_0} and K is illustrated in Fig. 20. The first step is to perform an initial screening using a full factorial, central-composite, or small-composite experimental design. After creating the experimental design, geometric constraints are applied to eliminate infeasible designs. With only geometrically feasible designs from which to choose, the D-optimality criterion is used to further reduce the size of the experimental design to an acceptable size.

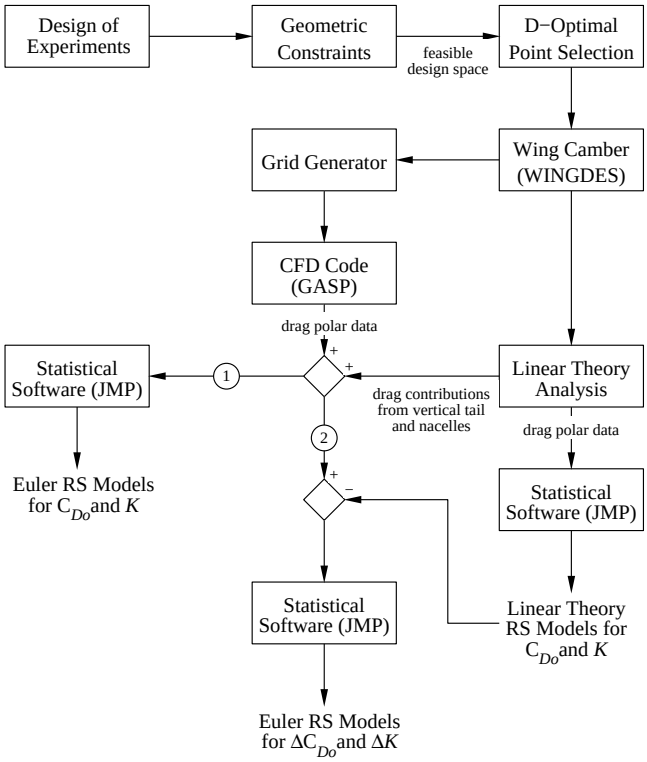

Figure 20: Flowchart for Creating RS Models.

WINGDES is used to provide a camber distribution for each of the D-optimal design points. The lift and drag are then computed from both linear theory and Euler analysis. Since the Euler calculations are only for wing–fuselage configurations, wave drag predictions for the vertical tail and nacelles from linear theory analysis are added to the Euler drag data. The values of C_{D_0} and K are computed using data from two points on the drag polar. Response surface models for C_{D_0} and K are found from the set of computational experiments using JMP.

A quadratic response surface model in m variables has the form

$$y = c_0 + \sum_{1 \leq j \leq m} c_j\, x_j + \sum_{1 \leq j \leq k \leq m} c_{jk}\, x_j\, x_k, \tag{7}$$

where y is the response, the x_j are the design variables, and c_0, c_j, and c_{jk} are the polynomial coefficients. There are $(m+1)(m+2)/2$ coefficients for a quadratic response sur-

face model in m variables, requiring a minimum of $(m+1)(m+2)/2$ design calculations to evaluate them. Studies by Giunta[43] *et al.* reveal that using approximately twice the minimum number of required points is sufficient to accurately compute the value of the coefficients for problems with five variables. However, as the dimension of the problem increases, the ratio of the number of points to the number of terms p/m in the response surface also increases. A systematic increase from $p/m = 2.0$ in the five variable case to $p/m = 3.5$ in the twenty variable case is used to provide adequate information for accurate RS modeling. This translates to 60, 276, 720, and 1470 CFD evaluations per RS model for the 5, 10, 15, and 20 variable problems, respectively. To compute the coefficients for the quadratic RS models of both C_{D_0} and K for a 30 variable problem would require 4184 CFD evaluations. On a single processor of the SGI *Power Challenge* R8000, this would require over 46 days of computation! Clearly, a method must be developed which enables accurate response surface estimates with a reduced number of required CFD analyses.

A.4. Reduced Term RS Models

Linear theory RS models can be readily created for moderately high dimensional spaces because the evaluations are so computationally inexpensive. Regression analysis, performed to obtain the coefficients of the polynomial models, also provides a means of systematically removing terms[38] from the RS models that have little or no impact on the response through a process called *stepwise regression analysis*. Terms are eliminated using a measure of the significance level of the term called the p-value. This represents the probability that the coefficient of a particular term is actually zero, not the value computed. Typically, a p-value of 0.05 or less indicates that the term is significant in predicting the variation in the response. As the prescribed value of the p-value is reduced, more terms are eliminated from the RS model. At some point in the stepwise regression process, the error in the RS model fit increases noticeably, indicating that too many terms have been eliminated in order to satisfy the p-value limit. For this research, the statistical package JMP[39] is used to perform the stepwise regression analysis.

The root mean square (RMS) error estimate is used to indicate the error in the RS model fit. The RMS error is calculated as

$$\text{RMS error} = \sqrt{\frac{\sum_{i=1}^{N} (y_i - \hat{y}_i)^2}{N}}, \tag{8}$$

where y_i is the observed value of the response and $\hat{y}_i$ is the predicted value of the response at the N sample points. The N sample points are a randomly selected subset of the points used in the initial screening experimental design not including the design points used in the creation of the RS models.

The stepwise regression technique is applied to the RS models for the linear theory aerodynamics to create *reduced term* RS models. Since the Mach 2.4 cruise regime is predominantly linear, performing regression analysis on the RS models for the linear theory aerodynamics should give a polynomial with nearly the same terms as the reduced term RS models for the Euler aerodynamics. Instead of creating quadratic RS models for the Euler results, one needs only to create the reduced term models found using linear theory analyses. Computational time is therefore not wasted evaluating coefficients which do not have a significant effect on the response.

The approach to implementing the reduced term models uses reduced term RS models for the difference between the Euler and linear theory RS model predictions, ΔC_{D_0} and ΔK To estimate the Euler values of the response, these *correction* RS models are added to the full term quadratic linear theory RS models. The sum of the linear theory and correction RS models will be referred to as the *incremental* RS models (*i.e.*, n term incremental RS model = full term linear theory RS model + n term correction RS model). These results are presented in Chapter 5.

B. Parallel Computing

Over one thousand CFD drag solutions are required to create the RS models and evaluate the errors for the 15 variable and 20 variable designs. Performing these calculations on a single processor of the SGI *Power Challenge* R8000 machine takes nearly two weeks of wall clock time. This time can be reduced significantly by taking advantage of parallel computing.

A coarse-grained parallelization of the CFD analyses has been implemented on the 119 node, distributed memory Intel *Paragon* XP/S at Virginia Tech. While fine-grained parallelization offers potentially better performance, especially for large numbers of nodes, coarse-grained parallelization is easier to implement and does not require in-depth knowledge of or modifications to the complex codes used. The parallel computations are organized in a "master-slave" paradigm, where one processor creates the directory structure and input files, distributes the jobs, and checks for their completion. Each individual CFD calculation is performed entirely by a single "slave" node.

Two measures of parallel performance are presented: the parallel speedup and efficiency. Speedup represents

the ratio of the serial calculation time to the parallel computation time on n_p nodes. The parallel efficiency is the speedup divided by the number of nodes. Ideally, the speedup equals the number of nodes, bringing the efficiency to 1.0; however, this ideal behavior is not realized. File I/O, which is inherently serial, increases with n_p and prevents the user from approaching ideal speedup and efficiency for large numbers of nodes. Reading and writing of input files, CFD grid files, and CFD solution files are examples of the file I/O present in the procedure.

In spite of these detractors, good performance is achieved when implementing the CFD calculations in parallel. Figure 21 shows the parallel speedup and efficiency obtained from performing 1080 CFD calculations for 360 HSCT configurations used in the 15 variable design. When using 27 nodes, a speedup of 24.3 (0.90 efficiency) is realized. When using 53 nodes, a speedup of 45.4 (0.86 efficiency) is achieved. Even though a single processor of the Intel *Paragon* is about ten times slower than a single processor of the SGI *Power Challenge*, significant improvements in the turn-around time are achieved when using a large number of nodes. On 53 nodes, the 1080 Euler calculations require only 2.8 days to complete.

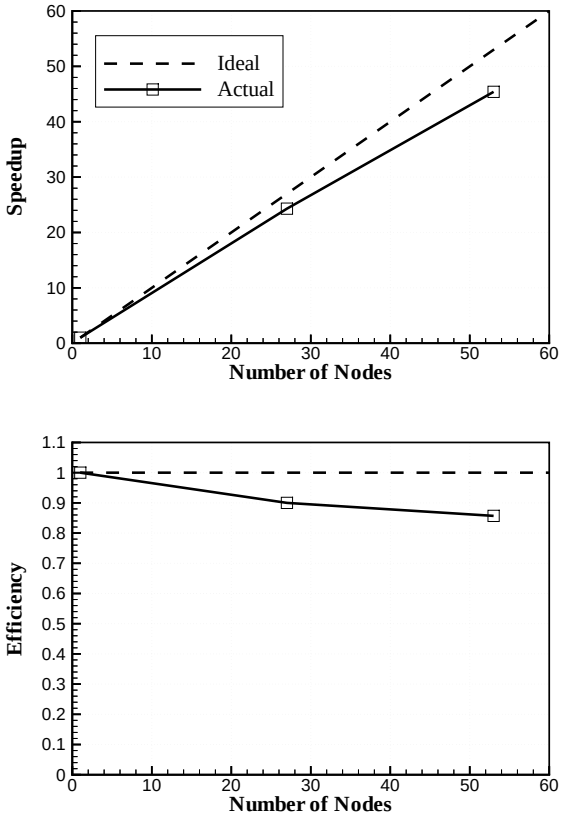

Figure 21: Parallel Speedup and Efficiency

C. Design Trade-offs and Sensitivities

Parametric studies are invaluable to a designer. These studies provide information on trade-offs between various disciplines and influences, sensitivities to variations in design variables, and effects of perturbations to a chosen design. To perform a single parametric study, 25–50 analyses may be required. To completely examine a design, many of these parametric studies would be desired. The computational burden involved in performing these numerous studies is greatly reduced by using results from RS models instead of data from a large number of CFD calculations since the expense lies only in the evaluation of the simple quadratic polynomials. In this section, we examine variations in selected design variables to gain insight into the behavior and relative importance of these parameters.

The optimal designs predicted from linear theory and Euler RS models for the five, ten, and fifteen variable design problems show the effects of the higher drag predictions typical of the supersonic Euler solutions. The thickness-to-chord ratio, t/c, is a direct trade-off (Fig. 1) between aerodynamics and structures. Aerodynamics dictates that the wing should be as thin as possible to reduce the drag and therefore the fuel weight. Structural optimization, on the other hand, would attempt to increase the thickness of wing to reduce the wing weight. A compromise is met between the fuel weight and wing weight to obtain the minimum TOGW. The effects of replacing the linear theory aerodynamics with Euler solutions is apparent in the fuel weight. The higher drag from Euler analysis translates to higher fuel weights and a design in which the aerodynamic aspects are more dominant. The optimal design is obtained at a lower t/c value to counter the effects of the higher drag at the expense of the wing weight.

The linear theory curve for the fuel weight variation with t/c has a nearly zero slope at $t/c = 1.5\%$. This occurs because the fuel weight required to meet the range constraint is not influenced only by the aerodynamics. As the wing gets thinner and the wing weight increases, there is a point where the fuel weight penalty associated with the increasing weight of the aircraft becomes as important as the fuel weight benefit from the reduced the drag. This point occurs near $t/c = 1.5\%$ when using linear theory analysis. When using Euler analysis, the fuel weight is still dominated by the aerodynamic benefits over the range of t/c investigated.

The decreased inboard leading-edge sweep in the optimal design from Euler aerodynamics is an interesting occurrence. This is not a result of aerodynamic–structural trade-offs, but rather it is due mainly to a compromise

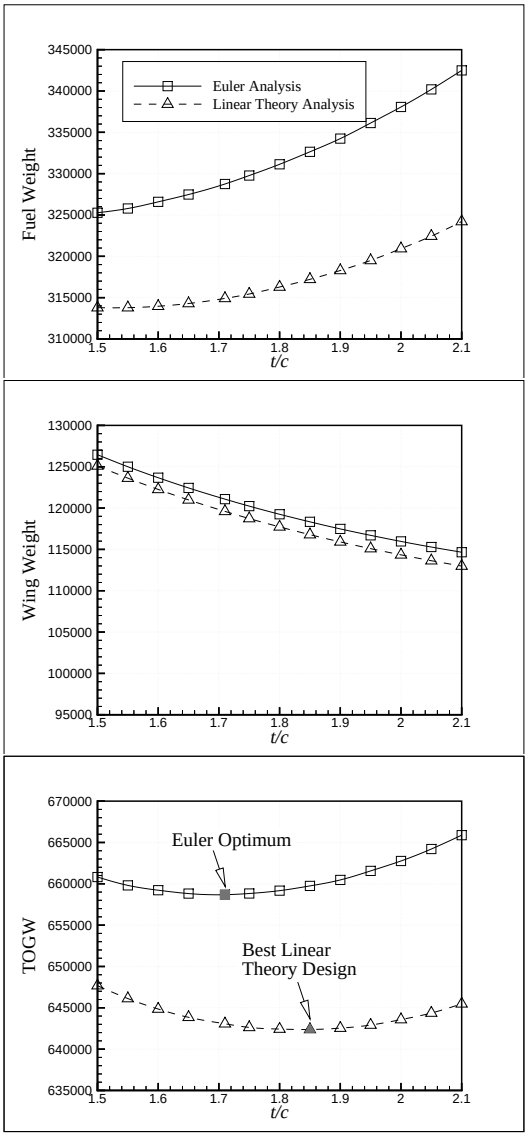

Figure 1: Aerodynamic–Structural Trade-Off for t/c.

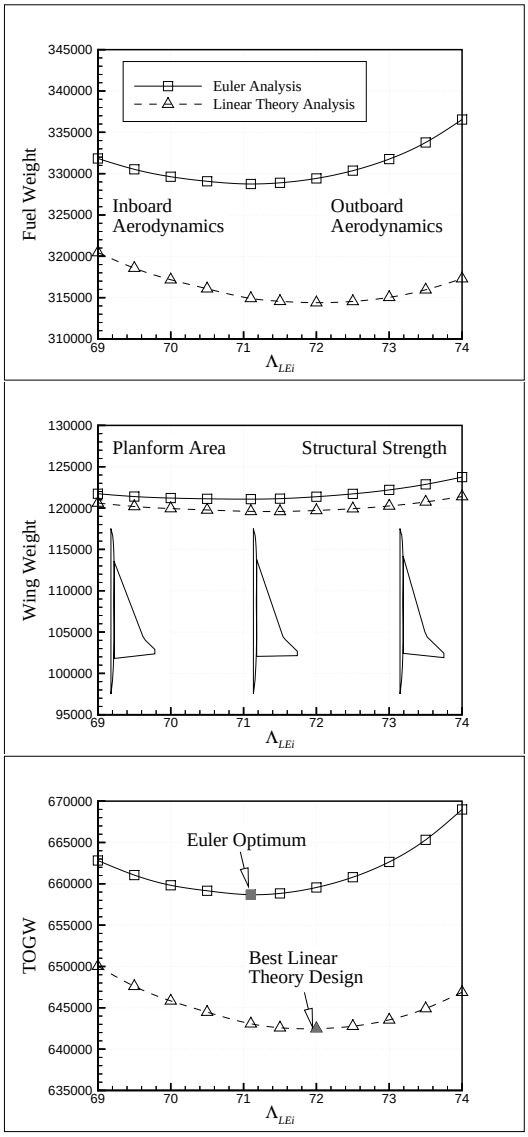

Figure 2: Trade-Off Study for Λ_{LE_I}.

between aerodynamic influences. With the semispan, $b/2$, and inboard LE length, s_{LE_I}, fixed, there is an increase in the size of the outboard section implicit with any increase in Λ_{LE_I}. The aerodynamic trade-off (Fig. 2) is between the high inboard sweep desired for improved supersonic performance and the size of the outboard section, which has poor supersonic performance. The nonlinear aerodynamic predictions have a relatively larger fuel weight penalty associated with the outboard section than do the linear theory results. This naturally shifts the optimal Λ_{LE_I} to a lower value.

The wing weight plot in Fig. 2 shows a Λ_{LE_I} compromise between structural effects as well. At the lowest wing sweep, the planform takes on a structurally sound shape. However, the large planform area results in extra weight. At the other extreme, the planform area is reduced, but the design is not as sound structurally. Extra weight is required to strengthen the structure. The best design is a trade-off between these two influences.